



## Article

# Identification of Fungicide Combinations Targeting *Plasmopara viticola* and *Botrytis cinerea* Fungicide Resistance Using Machine Learning

Junrui Zhang \* and Sandun D. Fernando \*

Biological and Agricultural Engineering Department, Texas A&M University, College Station, TX 77843-2117, USA  
\* Correspondence: zjr1996@tamu.edu (J.Z.); sfernando@tamu.edu (S.D.F.)

**Abstract:** Downy mildew (caused by *Plasmopara viticola*) and gray mold (caused by *Botrytis cinerea*) are fungal diseases that significantly impact grape production globally. Cytochrome b plays a significant role in the mitochondrial respiratory chain of the two fungi that cause these diseases and is a key target for quinone outside inhibitor (QoI)-based fungicide development. Since the mode of action (MOA) of QoI fungicides is restricted to a single active site, the risk of developing resistance to these fungicides is deemed high. Consequently, using a combination of fungicides is considered an effective way to reduce the development of QoI resistance. Currently, there is little information available to help in the selection of appropriate fungicides. This study used a combination of in silico simulations and quantitative structure–activity relationship (QSAR) machine learning algorithms to screen the most potent QoI-based fungicide combinations for wild-type (WT) and the G143A mutation of fungal cytochrome b. Based on in silico studies, mandestrobin emerged as the top binder for both WT *Plasmopara viticola* and WT *Botrytis cinerea* cytochrome b. Famoxadone appeared to be a versatile binder for G143A-mutated cytochrome b of both *Plasmopara viticola* and *Botrytis cinerea*. Thiram emerged as a reasonable, low-risk non-QoI fungicide that works on WT and G143A-mutated versions of both fungi. QSAR analysis revealed fenpropidin, fenoxanil, and ethaboxam non-QoIs to have a high affinity for G143A-mutated cytochrome b of *Plasmopara viticola* and *Botrytis cinerea*. Above-QoI and non-QoI fungicides can be considered for field studies in a fungicide management program against *Plasmopara viticola*- and *Botrytis cinerea*-based fungal infections.

**Keywords:** cytochrome b; QoI fungicides; fungicide resistance; QSAR; machine learning; grapes; downy mildew; gray mold



**Citation:** Zhang, J.; Fernando, S.D. Identification of Fungicide Combinations Targeting *Plasmopara viticola* and *Botrytis cinerea* Fungicide Resistance Using Machine Learning. *Microorganisms* **2023**, *11*, 1341. <https://doi.org/10.3390/microorganisms11051341>

Academic Editor: Wolf-Rainer Abraham

Received: 8 March 2023  
Revised: 11 May 2023  
Accepted: 13 May 2023  
Published: 19 May 2023



**Copyright:** © 2023 by the authors. Licensee MDPI, Basel, Switzerland. This article is an open access article distributed under the terms and conditions of the Creative Commons Attribution (CC BY) license (<https://creativecommons.org/licenses/by/4.0/>).

## 1. Introduction

Grapes, one of the most valuable cash crops, play an important role in the global economy. In 2020, the global production of grapes was 78 million tonnes from 6.95 million hectares, and the total production value was over USD 80 billion [1], with ~6 million tons of grapes produced in the U.S. [2]. Cultivated grapes are sold as table grapes and processed grape products such as jam, wine, vinegar juice, and jelly. Over 50% of grapes are used in wine production, which contributes to over a billion U.S. dollars each year in the U.S. However, fungal diseases have a serious impact on the growth of grapes, which also affects the quality of wine and other products. An estimated 40% reduction in grape production occurs annually because of various fungal diseases, causing significant economic losses [3].

Downy mildew caused by *Plasmopara viticola* is one of the most serious fungal diseases that attack grapevines. Downy mildew is a native pathogen to North America and caused serious damage to European vineyards in the late 1800s [4]. *Plasmopara viticola* invades leaves, shoots, and young berries under warm and moist conditions, allowing the pathogen to take nutrients from these parts to produce sporangia, causing larger infections [4,5]. Yellow spots with white downy mold occur on the surfaces of infected leaves, and the spots

turn brown and eventually necrotic [6]. Necrotic areas on leaves caused by downy mildew largely affect the photosynthesis of the grapevine and reduce the formation of glucose provided by photosynthesis, which hinders grape growth and causes a reduction of berries. Young shoots and berries are also vulnerable to downy mildew, which causes young shoots to become twisted and decreases the translocation of water and organic nutrients, slowing growth [6]. This infection also causes berries to dry out and fall, resulting in significant losses [6]. When there is abundant rainfall in warm seasons, the pathogen easily invades grapevines and reproduces more sporangia, which can be carried by wind or rain to infect surrounding grapevines [6,7]. Although downy mildew is devastating, QoI fungicides have thus far been able to manage the disease effectively [6–8]; however, a key mutation in the target results in resistance to several of these fungicides.

Gray mold caused by *Botrytis cinerea* is another fungal disease that causes serious destruction to grapevines. Gray mold is also one of the “Top 10 fungal plant pathogens” in the survey established by *Molecular Plant Pathology* because this fungal disease has a wide host range and can invade a host plant in all stages, from seedling to maturity [9]. The berries of grapevine are the most susceptible when an infection occurs at moderate temperatures and high humidity [10]. When the berries are infected, a reddish-brown and watery decay can be observed from the pedicel to the stylar end [10]. Infected regions also provide favorable conditions for a secondary inoculum, which will generate more sporangia and infect other berries nearby [10]. Infected berries finally dry out, resulting in significant economic losses. *Botrytis cinerea* also invades leaves, flowers, and shoots, causing similar brown lesions on plant parts [10]. QoI fungicides are commonly used for chemical control of *Botrytis cinerea* [10], and resistance threatens the effectiveness of several of these fungicides.

#### Literature Review

The application of fungicide is a chemical control that targets specific molecules such as amino acids to block fungal metabolism, restricting fungal reproduction [11]. The binding target of QoI fungicides is cytochrome b, a protein within the cytochrome bc<sub>1</sub> complex in *Plasmopara viticola* and *Botrytis cinerea* that plays a significant role in respiratory function [12]. When QoI fungicides bind cytochrome b, the ubiquinol oxidase substrate is unable to transfer electrons between cytochrome b and cytochrome c<sub>1</sub>, interrupting and inhibiting the production of adenosine triphosphate (ATP) [8,12]. This shortage of ATP interrupts the propagation of the pathogen, meaning downy mildew treated by QoI fungicides cannot infect other parts of the grapevine. However, since QoI fungicides are single-site fungicides (specifically binding to cytochrome b), downy mildew and gray mold will develop fungicide resistance after continuous usage of QoI fungicides [12–14]. Because of fungicide resistance development, the Fungicide Resistance Action Committee (FRAC) labeled QoI fungicides as high-risk. The G143A (glycine to alanine) mutation was the main known mutation that reduced the efficacy of QoI fungicides toward grape downy mildew because the mutation of this target site weakens the binding affinity between protein and the fungicides [12,15,16]. While developing new types of fungicides can resolve this issue, it takes a significant amount of time and resources to identify alternative active sites and undergo the rigorous approval processes. In the meantime, an effective, economical, and viable management strategy may include using combinations of fungicides. These combine one or more high-risk fungicides with one or more low-risk fungicides from those currently used [15]. With this strategy, QoI fungicides can be combined with another low-risk fungicide, providing the mixture with multiple binding targets and thus increasing the effectiveness against mutation [15].

Currently, only a few studies exist recommending fungicide combinations targeting *Plasmopara viticola* and *Botrytis cinerea* resistance, as summarized in Table 1. There is a gap in knowledge on what fungicide combinations should be selected to treat crops that have already developed resistance and also on what combinations would be most logical to use to prevent developing resistance. The approach we have taken in this study is to evaluate how

fungicides interact with WT and mutated versions of the target protein(s) at a molecular level to screen the highest-binding fungicides, which in turn will be recommended for field testing.

**Table 1.** Recent in vitro studies on fungicide combination recommendations targeting *Plasmopara viticola* and *Botrytis cinerea*.

Study	Results	Limitations
Field efficacy of the combination of famoxadone and metalaxyl-M against <i>Plasmopara viticola</i> and the residue dynamics of the two fungicides in grapevine [17].	Formulation of 30% famoxadone with metalaxyl-M SC was effective against <i>Plasmopara viticola</i> [17].	Only a few fungicides were tested in the experiment.
Performance and phytotoxicity assessment of mancozeb 40% + azoxystrobin 7% OS against downy mildew of grapes in Maharashtra, India [18].	Formulation of 40% mancozeb with 7% azoxystrobin was effective against <i>Plasmopara viticola</i> [18].	Only a limited number of fungicides were tested over a period of two years.
Evaluation of synergistic activity and resistance development of the mixture of iprodione and fluopyram against <i>Botrytis Cinerea</i> [19].	Formulation of 80% iprodione with 20% fluopyram was effective against <i>Botrytis cinerea</i> [19].	Only two fungicides were tested in this research.
Bioefficacy of different fungicides against <i>Plasmopara viticola</i> and <i>Erysiphe necator</i> of grapes [20].	Formulations of 16.6% famoxadone with 22.1% cymoxanil, 10% famoxadone with 50% mancozeb, and 4.44% fluopicolide with 66.67% fosetyl-AI were recommended for <i>Plasmopara viticola</i> [20].	Experiments were limited to existing fungicide combinations on the market.
Synergy between Cu-NPs and fungicides against <i>Botrytis cinerea</i> [21].	Formulation of copper nanoparticles with fluazinam or thiophanate was effective against <i>Botrytis cinerea</i> [21].	The study was limited to a select few fungicides, and the long-term efficacy is unknown. The development of effective new nanoparticles would require many years, and the process of producing copper nanoparticles would be challenging.

Select studies on fungicide combinations are shown in Table 1. A key limitation is that, since the studies were experimentally based, only a limited number of fungicides could be tested. Moreover, the long-term efficacy of these combinations is yet to be determined. A key advantage of in silico-based methods is their ability to screen a large number of fungicides simultaneously based on rational molecular-level information and select those with the highest promise for field testing. According to the existing literature, no studies have provided guidance for the selection of fungicide combinations based on molecular structures and their affinity for the target active site.

The significance of this work is that, as of now, there is only limited information for researchers to follow on selecting fungicides for *Plasmopara viticola* and *Botrytis cinerea* once resistance to existing fungicides is suspected. Also, there is no objective way to suggest fungicide combinations to reduce the development of resistance or treat crops that have already developed fungicide resistance. This study aims to provide a thermodynamic-coupled machine learning strategy to identify and select antifungal agents from QoIs (high-risk group) combined with low-risk fungicides to form fungicide combination(s) that can mitigate fungicide resistance. This approach is based on docking selected fungicides from QoIs and low-risk fungicides with a homology model of cytochrome b to identify the fungicides with the highest affinity and evaluating the screened fungicides using QSAR models with machine learning statistical methods.

## 2. Materials and Methods

### 2.1. Protein Structure and Ligand Structure Preparation

A homology model in PDB format of *Plasmopara viticola* (GenBank: DQ209286.1) was created using cytochrome b from plant mitochondrial complex III2 from *Vigna radiata* (PDB: 7JRG. 1 .C) as a template on the SWISS-MODEL server [11,22–24]. The quality of this homology model was evaluated using the programs ERRAT and PROVE on the SAVES v6.0 server [25,26]. The homology model contained G143 and F129, which were forms of WT cytochrome b. This model was mutated into G143A-mutated versions by Maestro Schrödinger. The canonical SMILES formulas of ligands were obtained from ZINC15 or PubChem (all 2D ligand structures are provided in Supplementary Materials Table S1), and the 3D structures of these ligands were generated in PDB format using the online SMILES translator [27,28]. All the protein and ligand structures were prepared for docking using the Protein Preparation Wizard, which added missing hydrogens, corrected bond orders, fixed missing segments, and minimized the structure under the Optimized Potentials for Liquid Simulations 3 (OPLS3) force field [29].

A homology model was built and validated for *Botrytis cinerea* using methods analogous to those developed for *Plasmopara viticola*.

### 2.2. Molecular Docking

Schrödinger Glide was used for the docking of the ligands on the protein. The grid box was centered around the original active sites (G143 and F129; coordinates X—195.53, Y—213.29, Z—176.3) or mutated active sites (G143A: coordinates X—192.6, Y—212.54, Z—171.55) and the size of the grid box was 44 × 46 × 56 Å. Glide docking scores between cytochrome b and the 27 ligands (ubiquinol and compounds 1–26 in Table S1) were generated using Schrödinger Glide XP mode with default settings in three replicates, and the highest binding scores were used for binding affinity analysis. The ligand-protein interactions were analyzed using a ligand interaction diagram.

### 2.3. AutoQSAR Model Analysis

In order to evaluate the predictions made by the docking, the Schrödinger automated quantitative structure–activity relationship (AutoQSAR) model with a machine-learning approach that is a subset of Artificial Intelligence (AI) was used. The AutoQSAR model is a machine-learning approach that builds numerical models with minimal inputs to interpret the relationship and make predictions between the bioactivity and chemical properties of ligands [30]. In this case, the binding affinity was used as the input variable. Numerical models were developed using multiple linear regression (MLR), partial least-squares regression (PLS), kernel-based partial least-squares regression (KPLS), and principal components regression (PCR) based on the given ligands' fingerprints, including linear, radial, dendritic, and milprint2D, or descriptors [30]. The AutoQSAR split the selected ligands into a 75% training set and a 25% test set for *Plasmopara viticola* and *Botrytis cinerea* [30]. This model generated a scatter plot that showed the correlation between observed and predicted binding affinity. The accuracy of this model was evaluated by an external validation data set.

More information on the fungicides that were used in the in silico study is given in Table 2. The structural information of the compounds used in both in silico and QSAR studies is given in Table S1.

**Table 2.** Resistance and mode of action information for fungicides selected in this study.

Fungicide	Resistance <sup>1</sup>	Fungicide Type <sup>2</sup>
Ubiquinol	NA	NA
Famoxadone	HR	QoI
Azoxystrobin	HR/R	QoI
Fenamidone	HR	QoI
Coumoxystrobin	HR	QoI
Flufenoxystrobin	HR	QoI
Enoxastrobin	HR	QoI
Pyraoxystrobin	HR	QoI
Picoxystrobin	HR	QoI
Metiltetraprole	HR	QoI
Fenaminstrobin	HR	QoI
Pyribencarb	HR	QoI
Dimoxystrobin	HR	QoI
Triclopyricarb	HR	QoI
Metominostrobin	HR	QoI
Pyrametostrobin	HR	QoI
Mandestrobin	HR	QoI
Fluoxastrobin	HR	QoI
Pyraclostrobin	HR	QoI
Orysastrobin	HR	QoI
Folpet	LR	PHT
Ferbam	LR	DTC
Captan	LR	PHT
Mancozeb	LR	DTC
Ametoctradin	HR/R	QoI
Thiram	LR	DTC
Zineb	LR	DTC

<sup>1</sup> Resistance: NA, native; HR, high risk; LR, low risk for the resistance of fungicides. <sup>2</sup> Fungicide type: QoI, quinone outside inhibitor; DTC, dithiocarbamate; PHT, phthalimides.

### 3. Results

#### 3.1. Building of the Homology Models for *Plasmopara viticola* Cytochrome b

The homology model of *Plasmopara viticola* cytochrome b included the regions between residues 79 and 295 found by BLAST. The sequence identity was 69.59%, and the sequence similarity was 0.53 [24]. The Quaternary Structure Quality Estimate (QSQE) was 0.81 (with 0.7 as acceptable), indicating a high level of reliability. The Global Model Quality Estimate (GMQE) was 0.89, meaning the homology model had over half of the target sequence coverage [24]. The ERRAT value for the homology model was 93.5, which meant that the homology model had acceptable nonbonded atomic interactions [25]. Based on the PROCHECK report, 92.9% of residues (171 out of 217) were located in the most favored regions, 6.5% (12 out of 217) were located in the additional allowed regions, 0% were located in the generously allowed regions, and 0.5% (1 out of 217) were located in the disallowed regions [31]. The residue score provided by PROCHECK was 99.5%, which indicated that the conformation of the homology model of *Plasmopara viticola* cytochrome b was stable [32]. Based on favorable scores, this homology model was used for in silico studies.

### 3.2. Identification of the Active Site for *Plasmopara viticola*

During the initial docking, the homology model was divided into top (covering residues ARG79-TRY94, MET124-PHE180, and PHE245-MET295) and bottom sections (covering residues ILE95-PHE121 and SER181-ILE244). To identify the docking site in cytochrome b, two conserved regions around the center of the protein were picked from the top and bottom parts based on the existing literature [33]. Initial docking results and the site map shown in Figure 1 revealed the strong binding of probe molecules to the top region (covering residues ARG79-TRY94, ILE122-PHE180, and PHE245-MET295) of cytochrome b. Since the top region showed stronger binding and included the residue where the antifungal-resistant mutation occurred, this region was used for docking analyses in all subsequent steps. The key interactions of ubiquinol at the binding site are given in Figure 1. Cytochrome b had strong hydrophobic interactions with ubiquinol, which was also predominant between cytochrome b and the fungicides tested (Figure 1). Hydrogen bonding was also observed with ARG178 for WT cytochrome b. Ubiquinol formed strong hydrogen bonds with MET295 of the G143A-mutated type.

### 3.3. Fungicide Binding Behavior on *Plasmopara viticola* Cytochrome b

Since the focus of this study was to identify fungicides that were effective against WT and the G143A mutation of cytochrome b, a set of known antifungal agents were docked onto WT and G143A-mutated types of *Plasmopara viticola* cytochrome b. Here, the G143A mutation was specifically selected since it was reported to be most significant for antifungal resistance [33].

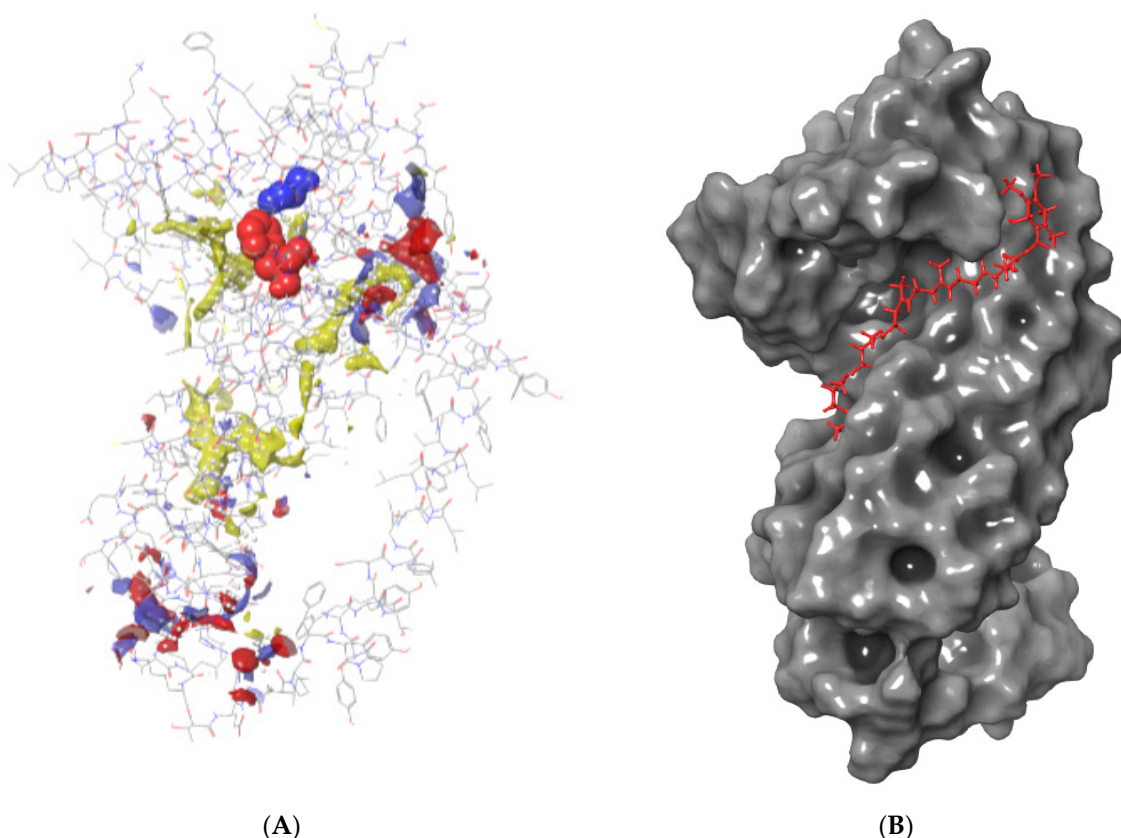
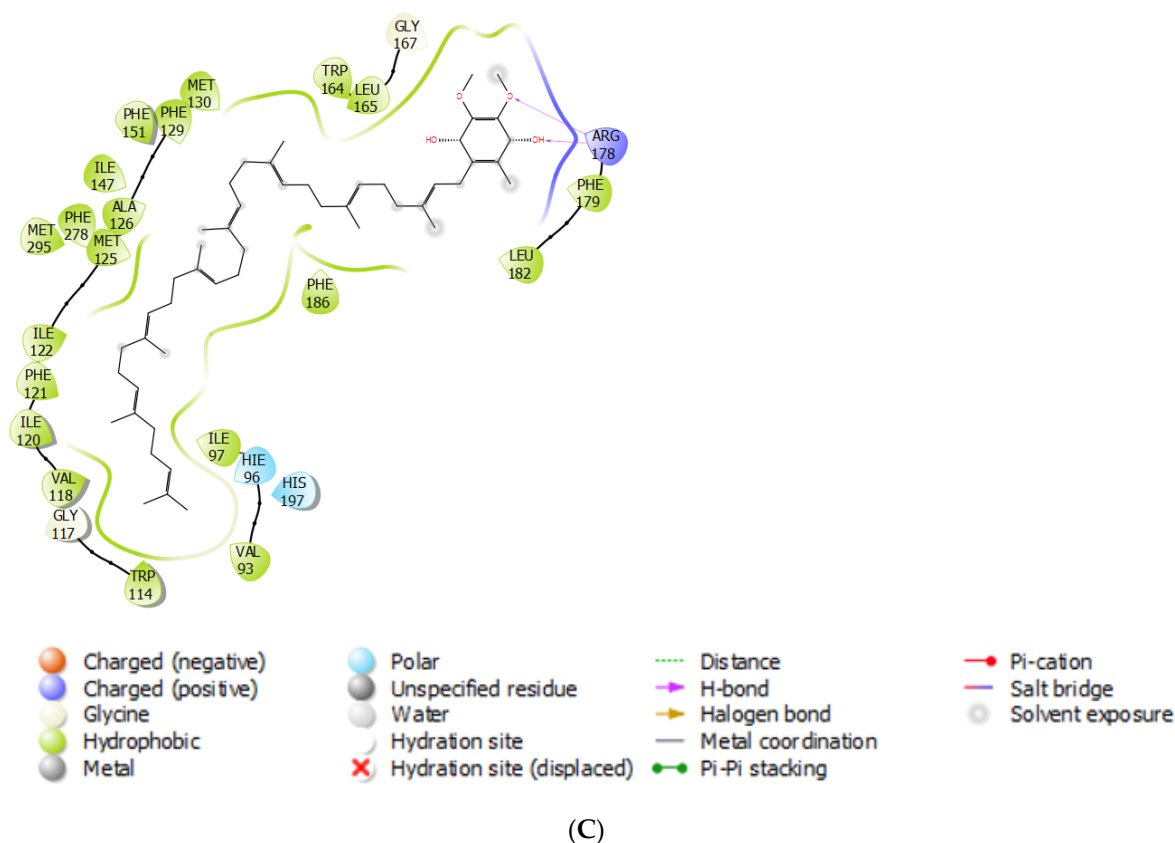


Figure 1. Cont.



**Figure 1.** (A) Site map output depicting possible binding sites of *Plasmopara viticola* cytochrome b (G143—blue residue; F129—red residue; hydrophobic—yellow areas; hydrogen-bonding acceptor—red areas; hydrogen-bonding donor—blue areas); (B) the top orientation of ubiquinol on cytochrome b (ubiquinol—red sticks; WT cytochrome b—gray surface); and (C) key interactions of ubiquinol with cytochrome b amino acid residues.

### 3.4. Mutation-Specific Observations

In order to reveal any specific interactions of fungicides with a particular mutation, the statistical analysis focused on each of the individual versions of *Plasmopara viticola* cytochrome b. This type of analysis will be helpful in identifying the best possible fungicide(s) if the mutation is known.

#### 3.4.1. Fungicide Recommendations for WT

In the case of WT, ubiquinol showed a strong binding affinity to WT cytochrome b (Figure 2), as expected. Mandestrobin, fenaminstrobin, dimoxystrobin, fenamidone, famoxadone, and ametoctradin had a stronger affinity than other high-risk fungicides, meaning they were effective agents for WT cytochrome b. Metominostrobin and thiram had higher affinities than the other fungicides, indicating that they were also effective against cytochrome b. Pyraoxystrobin, pyrametostrobin, pyraclostrobin, flufenoxystrobin, coumoxystrobin, picoxystrobin, triclopyricarb, oryastrobin, fluoxastrobin, and metylte-traprole did not bind to WT cytochrome b, and thus extensive usage of these fungicides has a high propensity to develop resistance. Azoxystrobin and ametoctradin are two fungicides known to be resistant to *Plasmopara viticola* [34,35]. Ametoctradin showed a somewhat strong affinity toward the WT version, although the docking score toward WT cytochrome b was lower than fenamidone, dimoxystrobin, fenaminstrobin, famoxadone, and mandestrobin. Azoxystrobin had a poor docking score, indicating that it may not be effective against cytochrome b inhibition. Among low-risk fungicides, i.e., fungicides having more than one MOA, thiram showed a strong affinity toward WT cytochrome b. Other low-risk fungicides such as captan, folpet, ferbam, and zineb did not bind tightly to WT cytochrome

b, which meant that these low-risk fungicides were not recommended because of their high potential susceptibility to resistance.

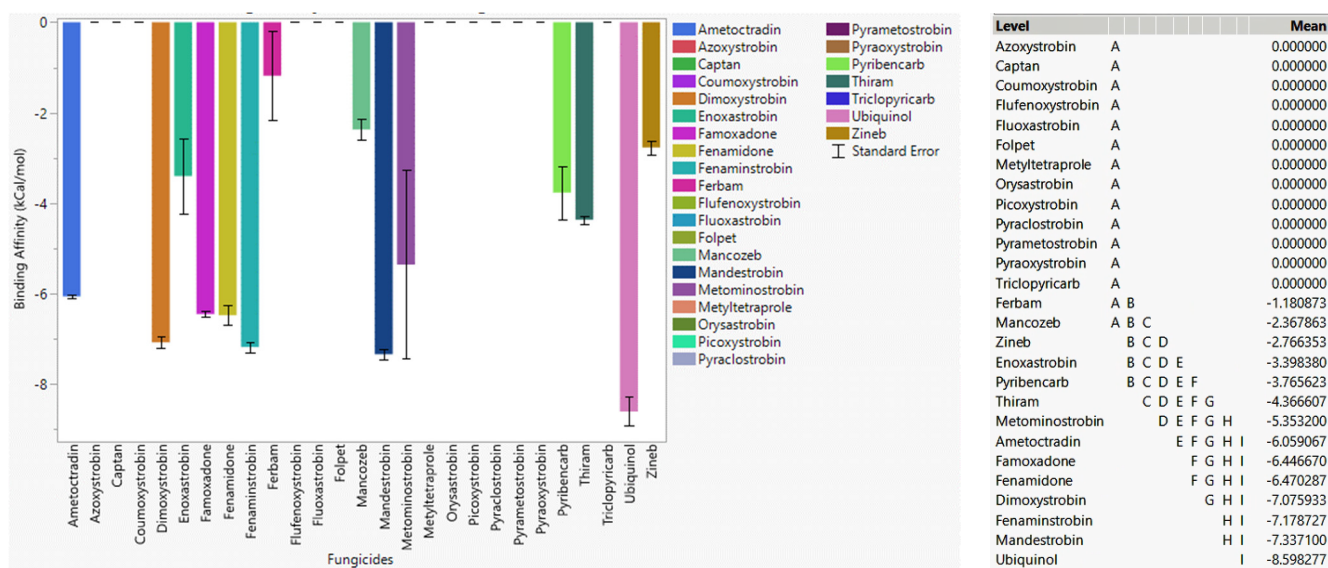


**Figure 2.** The performance of selected QoI fungicides on WT cytochrome b of *Plasmopara viticola* in a specific grid box. Mean—average binding affinity of three replicates (generated by Glide docking on Maestro Schrödinger) of the corresponding ligand; level—ligands with the same letter are not significantly different (letter level A: ligands with the lowest binding affinity; letter level I: ligands with the highest binding affinity).

### 3.4.2. Fungicide Recommendations for the G143A Mutation

Ubiquinol as a native substrate also showed a strong affinity for the G143A mutation of cytochrome b (Figure 3). Mandestrobin, fenaminstrobin, dimoxystrobin, fenamidone, famoxadone, and ametoctradin, which showed strong affinity toward WT cytochrome b and were effective agents against G143A-mutated cytochrome b. Coumoxystrobin, flufenoxystrobin, pyribencarb, and metominostrobin did not show a high binding affinity to WT cytochrome b, but they were effective fungicides when the G143A mutation occurred, meaning the interaction between the G143A-mutated version and those ligands was stronger than WT cytochrome b. Pyraoxystrobin, pyrametostrobin, pyraclostrobin, flufenoxystrobin, enoxastrobin, picoxystrobin, triclopyricarb, oryastrobin, fluoxastrobin, and metyltetraprole did not bind to G143A-mutated cytochrome b, indicating that these high-risk fungicides were not preferred for G143A-mutated cytochrome b. Low-risk fungicides folpet and thiram showed higher binding affinities than ferbam, zineb, mancozeb, and captan, which meant folpet and thiram would be more effective fungicides for G143A-mutated cytochrome b. As a resistant fungicide, azoxystrobin did not bind to either WT or G143A-mutated cytochrome b as expected.

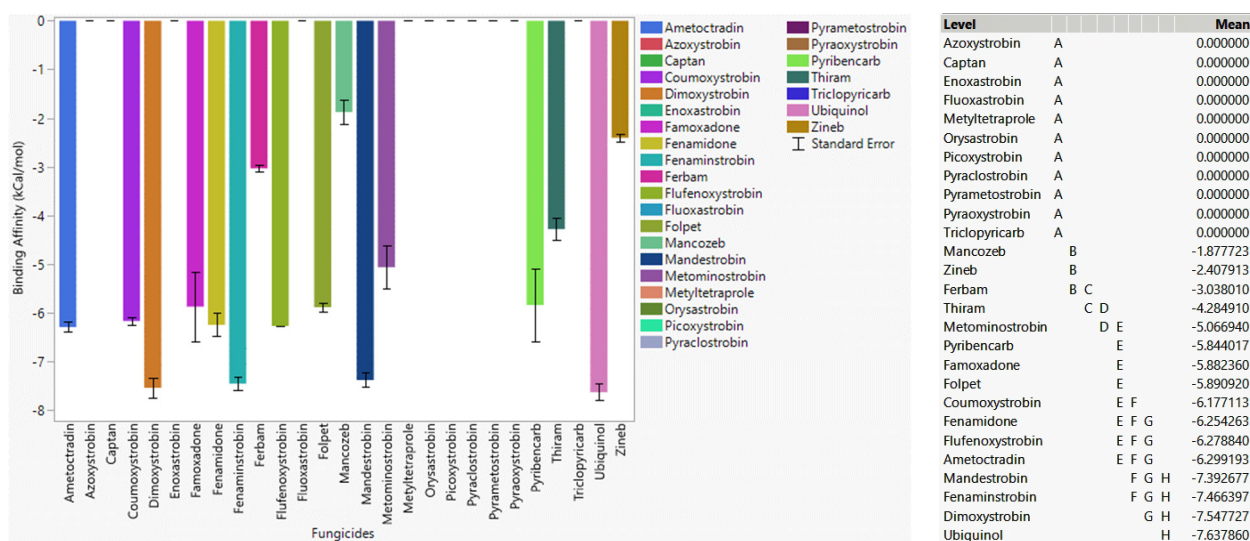


**Figure 3.** The performance of selected QoI fungicides on G143A-mutated cytochrome b of *Plasmopara viticola* in a specific grid box. Mean—average binding affinity of three replicates (generated by Glide docking on Maestro Schrödinger) of the corresponding ligand; level—ligands with the same letter level are not significantly different (letter level A: ligands with the lowest binding affinity; letter level H: ligands with the highest binding affinity).

A common recommendation is to use fungicide combinations that consist of different MOAs, i.e., combining one MOA with others in a fungicide rotation program. Because of their ability to tackle mutation, fenamidone, famoxadone, mandestrobin, dimoxystrobin, fenaminstrobin, ametoctradin, and thiram have been identified as suitable candidates for a rotational program targeting *Plasmopara viticola*.

The top conformation interactions of the highest affinity fungicides with G143A-mutated versions are given in Figure 4. Dimoxystrobin showed strong hydrophobic and hydrogen bonding interactions with MET125 of G143A-mutated cytochrome b. It was evident that the primary interactions between fungicides and cytochrome b were hydrophobic, which agreed with the predominantly hydrophobic nature of cytochrome b proteins [36,37]. Figure 4 shows dimoxystrobin forming strong hydrophobic interactions with the ILE122-ILE147 and PHE275-MET295 regions in the G143A-mutated versions. Of the low-risk fungicides, thiram showed strong hydrophobic interactions with cytochrome b.

Based on the binding analysis (Figure 5), the pocket located on the top region of cytochrome b that contained the residues F129 and G143 seemed to be an important binding position when targeting *Plasmopara viticola* inhibition. Ametoctradin, famoxadone, fenamidone, fenaminstrobin, mandestrobin, dimoxystrobin, metominostrobin, and thiram tended to bind to this pocket, including the native substrate ubiquinol.

### 3.5. Fungicide Binding Behavior on *Botrytis cinerea* Cytochrome b

To further verify binding affinities, an additional set of docking simulations were performed, this time using a grid box covering the ubiquinol binding site and the specific residues G143 and F129 on cytochrome b of *Botrytis cinerea*. For this analysis, the same 26 fungicides (Compounds 1–26 in Table S1), including resistant, high-risk, and low-risk, were selected. *Botrytis cinerea* was used because *Plasmopara viticola* was an obligate parasite and experimental validations could only be performed under field conditions, whereas *Botrytis cinerea* validations could easily be carried out in a laboratory setting.

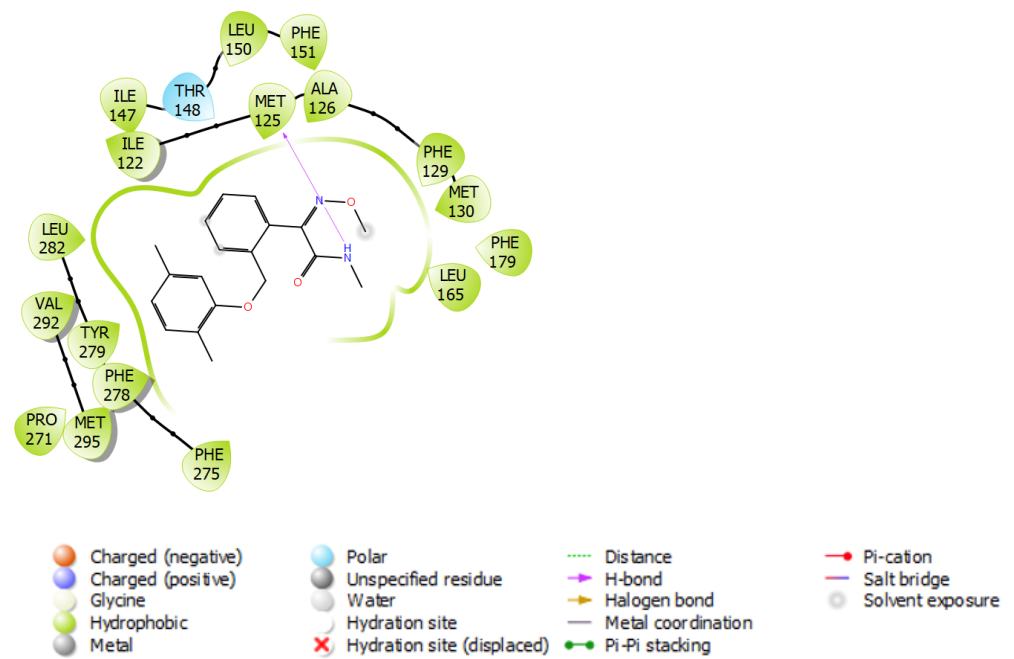


**Figure 4.** Binding interactions of dimoxystrobin with the G143A-mutated type of cytochrome b.

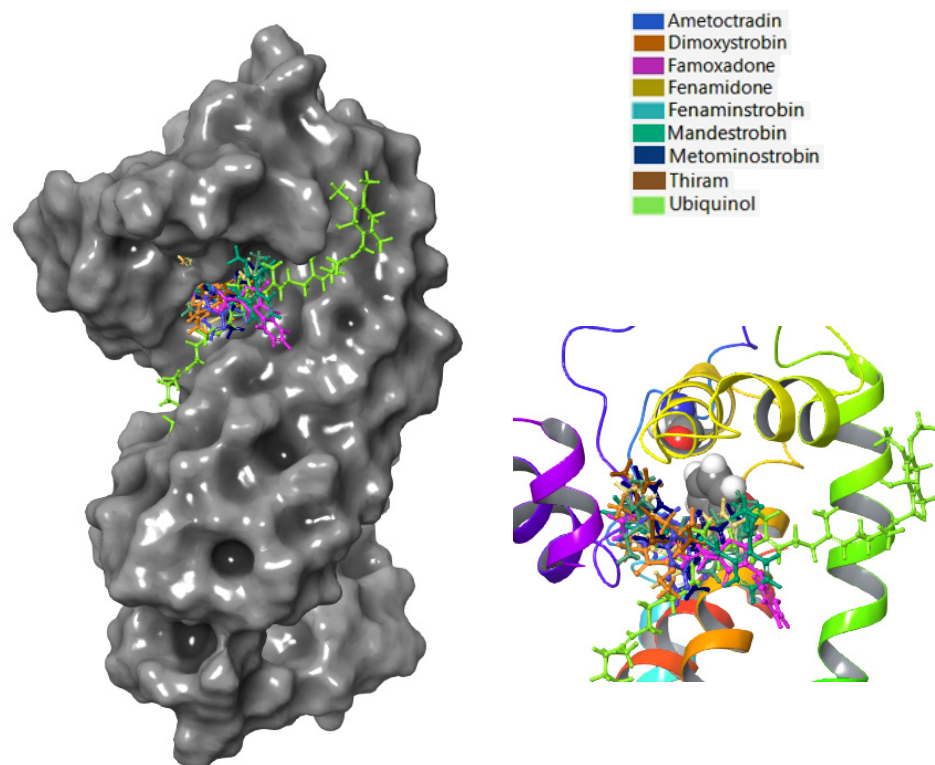


**Figure 5.** Ametoctradin, Famoxadone, Fenamidone, Fenaminstrobin, Mandestrobin, Dimoxystrobin, Metominostrobin, Thiram, and Ubiquinol are visualized as sticks of different colors bound to WT cytochrome b of *Plasmopara viticola*. Here, WT cytochrome b is represented as a gray surface, while different fungicides are depicted in different colors. The figure to the right represents a close-up of the active site, with the protein represented as a rainbow-colored ribbon and F129 and G143 represented as ball structures.

### 3.6. Mutation-Specific Observations

#### 3.6.1. Fungicide Recommendations for WT

It was observed that pyraoxystrobin, mandestrobin, enoxastrobin, and pyribencarb had higher binding affinity than ubiquinol to WT cytochrome b, indicating their potential superiority as effective fungicides via inhibition of cytochrome b of *Botrytis cinerea* (Figure 6). Fenaminstrobin, pyraclostrobin, dimoxystrobin, famoxadone, metominstrobin, pyrametostrobin, flufenoxystrobin, picoxystrobin, folpet, ametoctradin, fenamidone, captan, and triclopyricarb had higher affinities to WT cytochrome b than the other fungicides. Azoxystrobin, as an identified resistant fungicide, did not bind to WT cytochrome b. Coumoxystrobin, fluoxastrobin, metyltertrapole, and orysastrobin did not bind to WT cytochrome b, indicating their high likelihood of succumbing to resistance. Moreover, zineb and ferbam were low-risk fungicides that showed weaker binding affinity than captan, thiram, and folpet, which meant zineb and ferbam were not likely to be effective fungicides against cytochrome b of *Botrytis cinerea*.

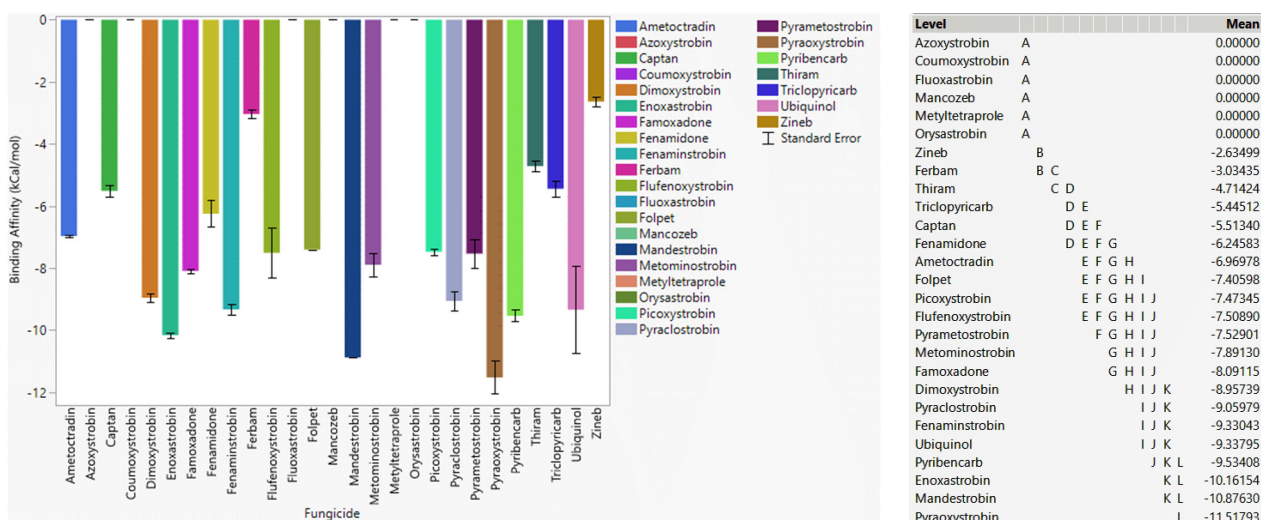


**Figure 6.** The performance of selected QoI fungicides on WT cytochrome b of *Botrytis cinerea* in a specific grid box. Mean—average binding affinity of three replicates (generated by Glide docking on Maestro Schrödinger) of the corresponding ligand; Level—ligands with the same letter level are not significantly different (letter level A: ligands with the lowest binding affinity; letter level L: ligands with the highest binding affinity).

#### 3.6.2. Fungicide Recommendations for the G143A Mutation

Fungicides famoxadone, mandestrobin, pyribencarb, picoxystrobin, metominstrobin, fenamidone, pyraoxystrobin, and thiram showed a stronger affinity to G143A-mutated cytochrome b of *Botrytis cinerea* than ubiquinol, indicating their superior ability to withstand the resistance caused by the G143A mutation of cytochrome b of *Botrytis cinerea* (Figure 7). Enoxastrobin, fenaminstrobin, flufenoxystrobin, and pyrametostrobin also showed a strong affinity toward WT cytochrome b but did not bind or bound weakly to G143A-mutated cytochrome b, meaning these fungicides may not be effective if the G143A mutation occurred. Coumoxystrobin, fluoxastrobin, metyltertrapole, and orysastrobin did not bind to G143A cytochrome b. Azoxystrobin, as an identified resistant fungicide, did not bind to G143A cytochrome b. Ferbam and zineb had weaker binding affinity, while captan and folpet did not bind to G143A cytochrome b, indicating that these four low-risk fungicides were not likely effective against G143A-mutated cytochrome b of *Botrytis cinerea*.



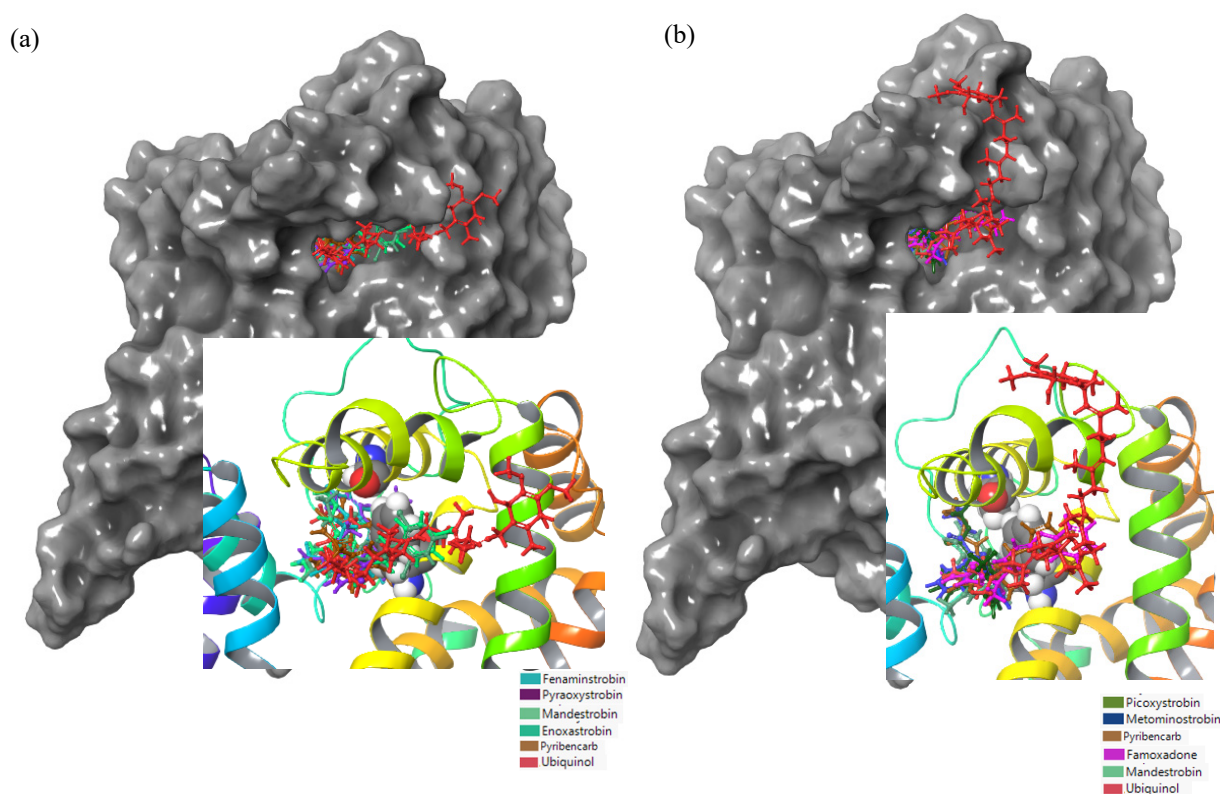


**Figure 8.** (a) Fenamidstrobin, Pyraoxystrobin, Mandestrobin, Enoxastrobin, Pyribencarb, and Ubiquinol with WT cytochrome b and (b) Picoxystrobin, Metominostrobin, Pyribencarb, Famoxadone, Mandestrobin, and Ubiquinol are visualized as sticks of different colors bound to G143A cytochrome b of *Botrytis cinerea*. Here, WT and G143A-mutated cytochrome b are represented as gray surfaces while different fungicides are depicted in different colors. The figure to the right represents a close-up of the active site, with the protein represented as a rainbow-colored ribbon and F129 and G143 or G143A represented as ball structures. The colors in the key are for stick models.

### 3.7. AutoQSAR Model Evaluation

#### Application of AutoQSR to Predict Fungicides for *Botrytis cinerea*

##### Training Data without a Validation Set

An initial training set was developed using 16 QoI and 18 non-QoI fungicides. The top five QSAR models and their performance parameters generated for *Botrytis cinerea* are depicted in Supplementary Figure S1, and these were pls\_19, kpls\_radial\_19, kpls\_dendritic\_19, kpls\_desc\_19, and kpls\_linear\_19. Based on the scoring functions, the best model was pls\_19, which was generated by partial least squares regression (PLS) using the 19th split of the learning set into a test and training set (34 ligands) without a validation set. This model had a standard deviation (S.D.) of 2.1184, a  $R^2$  of 0.6378, a root mean square error (RMSE) of 2.1419, a  $Q^2$  of 0.6172, and a ranking score of 0.5892. Binding affinity,  $Y(\text{Obs})$ , and predicted affinity,  $Y(\text{Pred})$ , from the QSAR model of all selected ligands are shown in Figure 10a (under DATASET) and Supplementary Figure S2, with 75% of the ligands belonging to the training set and 25% of the ligands to the test set for *Botrytis cinerea*. The five scatter plots in Figure 10 (b) and Supplementary Figure S3 were generated based on  $Y(\text{Obs})$  and  $Y(\text{Pred})$ . The results indicated that about 50% of training sets were close to the regression line.

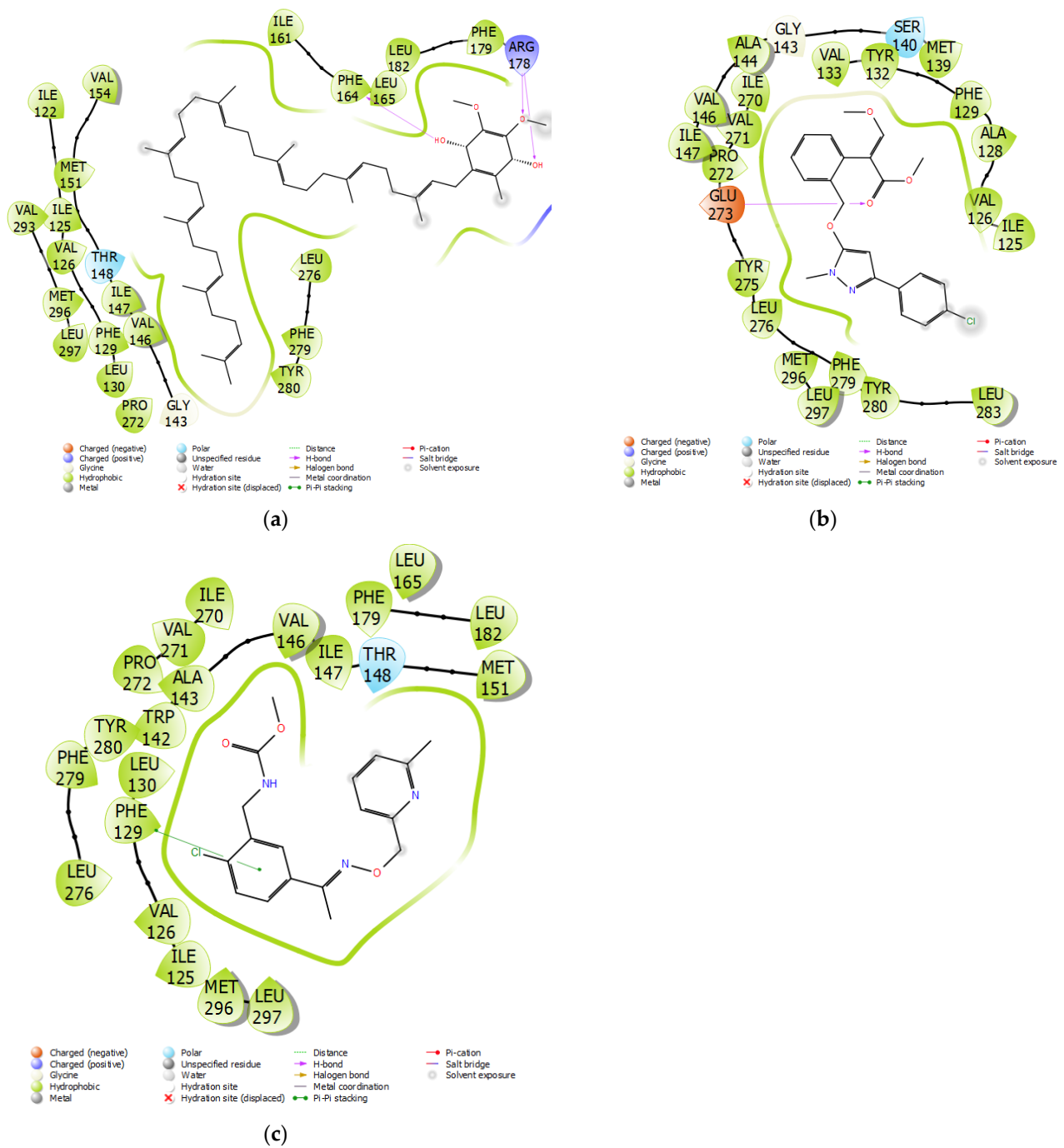
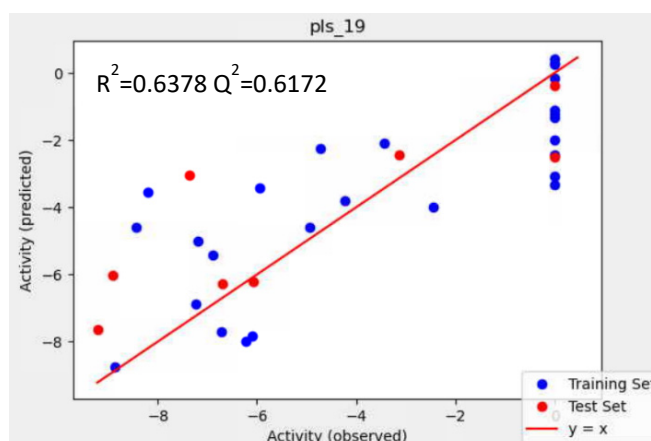


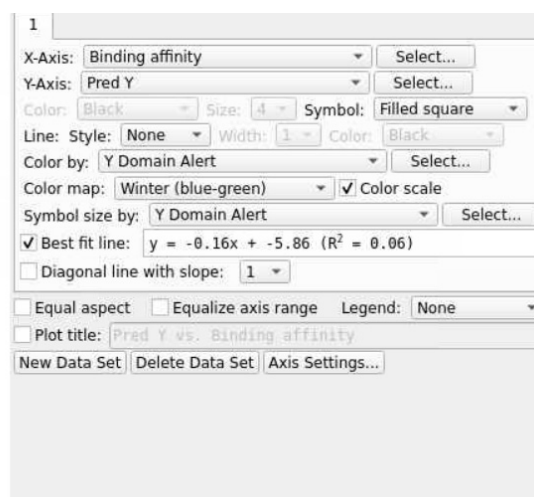
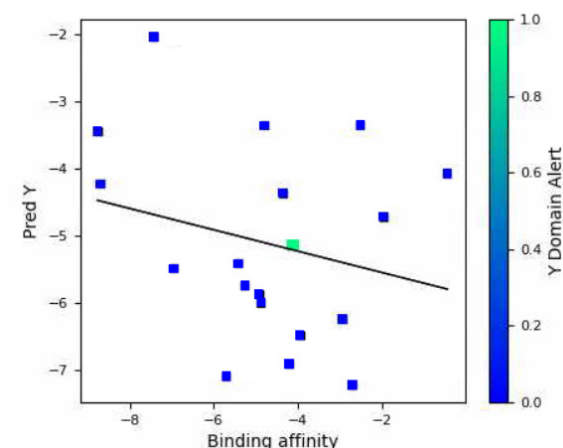
**Figure 9.** (a) Ubiquinol and (b) Pyraoxystrobin interactions with WT cytochrome b, and (c) Pyribencarb interactions with the G143A mutation of cytochrome b of *Botrytis cinerea*.

		Training Set		Test Set		
		S.D.	R <sup>2</sup>	RMSE	Q <sup>2</sup>	
		2.1184	0.6378	2.1419	0.6172	
Optimum number of factors = 2						
ID Set	Y(Obs)	Y(Pred)	Error	Name		
1 train	0.0000	-1.2316	-1.2316	Azoxystrobin		
2 train	0.0000	-1.0966	-1.0966	Coumoxystrobin		
3 train	-4.2340	-3.7908	0.4432	Dimoxystrobin		
4 test	0.0000	-0.3733	-0.3733	Enoxastrobin		
5 train	-5.9500	-3.4246	2.5254	Fenamidone		
6 train	0.0000	0.2465	0.2465	Fenaminstrobin		
7 train	0.0000	0.2781	0.2781	Fluoxastrobin		
8 train	0.0000	-3.0818	-3.0818	Metyltetraprole		
9 train	0.0000	-2.0068	-2.0068	Orysastrobin		
10 train	-8.2000	-3.5352	4.6648	Picoxystrobin		
11 train	-3.4420	-2.0826	1.3594	Pyraclostrobin		
12 train	0.0000	-3.3416	-3.3416	pyrametostrobin		
13 train	-4.7170	-2.2506	2.4664	Pyraoxystrobin		
14 train	-8.4460	-4.5987	3.8473	Pyribencarb		
15 test	0.0000	-2.5108	-2.5108	Triclopyricarb		
16 train	0.0000	-0.1531	-0.1531	Captan		
17 test	-3.1360	-2.4535	0.6825	Ferbam		
18 train	0.0000	0.4105	0.4105	Folpet		
19 train	0.0000	-1.3391	-1.3391	Mancozeb		
20 train	-4.9350	-4.5968	0.3382	Thiram		
21 train	-2.4520	-4.0030	-1.5510	Zineb		
22 train	-7.2440	-6.8650	0.3790	Zoxamide		
23 test	-9.2080	-7.6302	1.5778	Sedaxane		
24 test	-8.9120	-6.0174	2.8946	Piperalin		
25 train	-6.2170	-7.9841	-1.7671	Inpyrfluxam		
26 train	-8.8700	-8.7600	0.1100	Penconazole		
27 train	-6.0890	-7.8202	-1.7312	Ferimzone		
28 test	-7.3720	-3.0436	4.3284	Cyflufenamid		
29 test	-6.6920	-6.2838	0.4082	Diclomezine		
30 train	-7.2000	-5.0107	2.1893	Dichlobentiazox		
31 test	-6.0650	-6.2163	-0.1513	Ethaboxam		
32 train	-6.7210	-7.7085	-0.9875	Fluindapyr		
33 train	-6.8900	-5.4280	1.4620	Fluoxapiprolin		
34 train	0.0000	-2.4327	-2.4327	Flufenoxystrobin		



(a)

(b)



(c)

**Figure 10.** (a) Model report for the pls<sub>19</sub> model, (b) scatter plot providing the performance for the pls<sub>19</sub> model, and (c) scatter plot of the prediction set for the top QSAR models in Figure S1 for *Botrytis cinerea* without using a validation set.

In order to evaluate whether the predictions could be improved, it was decided to refine the models by systematically removing outliers that were chemically distinct from the ones that functioned as QoIs and/or when the difference between actual and predicted affinities was larger than 3 kCal/mol.

### Iteration #1

The new external validation set that included 19 ligands (Supplementary Table S2) was used to estimate the prediction accuracy of the QSAR model made by the top five numeric models listed in Figure S1. The  $R^2$  value of the best-fit line was 0.06, meaning the QSAR model was not able to predict with an acceptable level of accuracy for the given validation set. Moreover, some ligands in Figure 10c fell outside the applicability domain of the QSAR model, which would decrease the prediction accuracy of the QSAR model. Visual inspection of Figure 10c showed that metominostrobin, azaconazole, dithianon, and picarbutrazox were outliers, indicating these ligands were possibly unsuitable for the validation set for the built model. Both azaconazole and picarbutrazox had multiple heterocyclic nitrogen atoms (Table S1). Dithianon was the only ligand that contained heterocyclic dual sulfur atoms among the 19 ligands. Metominostrobin, azaconazole, dithianon, and picarbutrazox had an oxygen-containing aromatic ring, and there were at least two oxygen atoms in each ligand. The structural features mentioned above might be the reason these four ligands were not suitable for the validation set. To improve the prediction accuracy of the QSAR model, these ligands were considered for removal in the next iteration.

### Iteration #2

After removing metominostrobin, azaconazole, dithianon, and picarbutrazox, 15 ligands were next considered in the validation set (Table S2). The  $R^2$  value of the best-fit line increased from 0.06 to 0.26, indicating the four outliers might be potential factors affecting the prediction accuracy of the QSAR model. Both furametpyr and iprodione had chlorine in their chemical structure, which was similar to azaconazole, which was removed in first iteration (Table S1). Furametpyr, iprodione, and penthiopyrad had heterocyclic dual nitrogen atoms. Diethofencarb had a similar structure to metominostrobin, which was removed in the first iteration. Based on the visual inspection of Supplementary Figure S4 and similar chemical structures, furametpyr, iprodione, penthiopyrad, and diethofencarb were considered potential outliers.

### Iteration #3

After removing the eight outliers (metominostrobin, azaconazole, dithianon, picarbutrazox, furametpyr, iprodione, penthiopyrad, and diethofencarb) in this iteration, the  $R^2$  value in Supplementary Figure S5 of the best-fit line increased from 0.26 to 0.53. The rest of the compounds in Table S2 were more acceptable as an external validation set, meaning that they were expected to generate better predictions. The top predictions that would withstand G143A-mutated cytochrome b of *Botrytis cinerea* were fenpropidin (an amine), fenoxanil (a melanin biosynthesis inhibitor dehydratase), isoflucypram (a succinate dehydrogenase inhibitor), and ametocradin (a QoI). Although oxathiapiprolin and triazoxide had a high predicted binding affinity, their original affinity was low, so they were not acceptable. Chlorine and multiple heterocyclic nitrogen were considered similar to the outliers' structures.

### 3.8. Training Data with a Validation Set

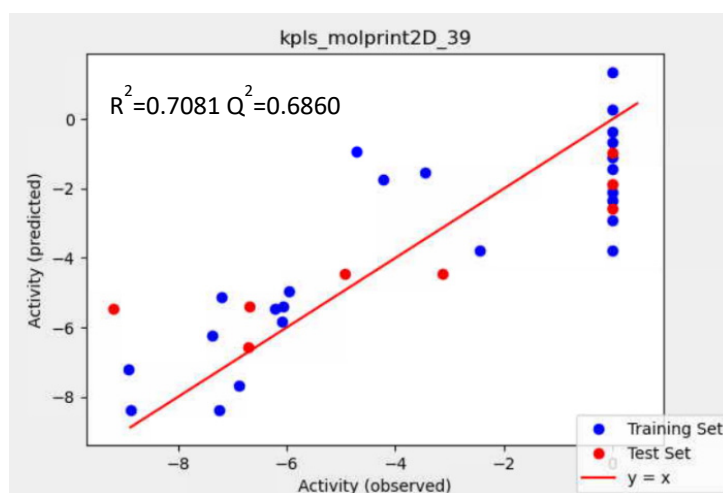
In this case, two QoI fungicides, picoxystrobin and pyribencarb, were assigned as a validation set for the QSAR models. This resulted in 32 ligands in the training set for the QSAR model (Figure 11a and Supplementary Figure S7). The ranking scores for the top five QSAR models with a validation set (Supplementary Figure S6) were higher than the model without the validation set, meaning that the test set predictions of a model with a validation set might be more accurate. The top QSAR models shown for *Botrytis cinerea* in Figure S6 were kpls\_molprint2D\_39, kpls\_radial\_8, kpls\_linear\_30, kpls\_dendritic\_30, and kpls\_dendritic\_39. The best model was kpls\_molprint2D\_39, which was generated by kernel partial least squares regression (KPLS) with molprint2D fingerprint, using the 39th split of the learning set into a test and training set (32 ligands) with the validation set (2 ligands). This model had an S.D. of 1.8732, a  $R^2$  of 0.7081, an RMSE of 1.8919, a  $Q^2$  of 0.6860, and a ranking score of 0.6582. As seen in the plots in Figure 11b and Supplementary

Figure S8, training sets were closer to the regression line (Figures 10b and S3), indicating the better prediction ability of the model.

Training Set				Test Set	
S.D.	R <sup>2</sup>	RMSE	Q <sup>2</sup>		
1.8732	0.7081	1.8919	0.6860		

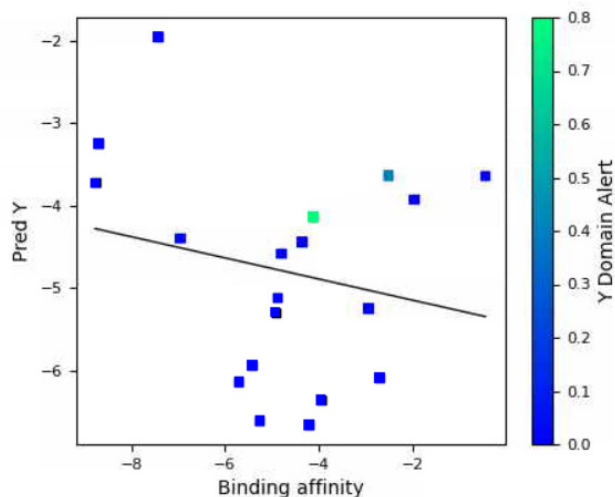
Optimum number of factors = 1

ID	Set	Y(Obs)	Y(Pred)	Error	Name
1	train	0.0000	-0.3674	-0.3674	Azoxystrobin
2	train	0.0000	0.2836	0.2836	Coumoxystrobin
3	train	-4.2340	-1.7477	2.4863	Dimoxystrobin
4	test	0.0000	-1.8764	-1.8764	Enoxastrobin
5	train	-5.9500	-4.9577	0.9923	Fenamidon
6	train	0.0000	-2.1022	-2.1022	Fenaminstrobin
7	train	0.0000	-1.4236	-1.4236	Fluoxastrobin
8	train	0.0000	-0.6732	-0.6732	Metiltetraprole
9	test	0.0000	-2.5727	-2.5727	Oryastrobin
10	train	-3.4420	-1.5155	1.9265	Pyraclostrobin
11	train	0.0000	1.3704	1.3704	pyrametostrobin
12	train	-4.7170	-0.9159	3.8011	Pyraoxystrobin
13	train	0.0000	-1.0953	-1.0953	Triclopyricarb
14	train	0.0000	-2.9122	-2.9122	Captan
15	test	-3.1360	-4.4439	-1.3079	Ferbam
16	train	0.0000	-2.3433	-2.3433	Folpet
17	train	0.0000	-3.7729	-3.7729	Mancozeb
18	test	-4.9350	-4.4439	0.4911	Thiram
19	train	-2.4520	-3.7729	-1.3209	Zineb
20	train	-7.2440	-8.3919	-1.1479	Zoxamide
21	test	-9.2080	-5.4768	3.7312	Sedaxane
22	train	-8.9120	-7.2108	1.7012	Piperalin
23	train	-6.2170	-5.4768	0.7402	Inpyrfluxam
24	train	-8.8700	-8.3718	0.4982	Penconazole
25	train	-6.0890	-5.8389	0.2501	Ferimzone
26	train	-7.3720	-6.2429	1.1291	Cyflufenamid
27	test	-6.6920	-5.3921	1.2999	Diclomezine
28	train	-7.2000	-5.1205	2.0795	Dichlobentiazox
29	train	-6.0650	-5.3898	0.6752	Ethaboxam
30	test	-6.7210	-6.5737	0.1473	Fluindapyr
31	train	-6.8900	-7.6645	-0.7745	Fluoxapiprolin
32	test	0.0000	-0.9534	-0.9534	Flufenoxystrobin



(a)

(b)



(c)

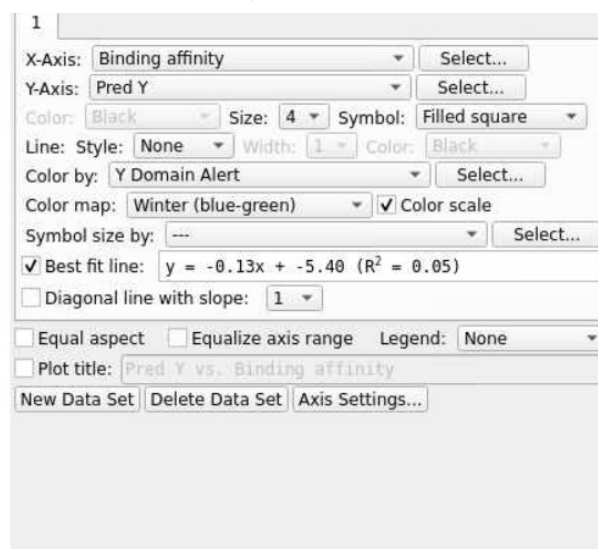


**Figure 11.** (a) Model report for the kpls\_radial\_39 model, (b) scatter plot providing the performance of the kpls\_radial\_39 model and (c) scatter plot of the prediction set for the top QSAR models in Figure S6 for *Botrytis cinerea* using a validation set.

Similar to the procedure that was adopted in the previous run, several iterations were conducted while removing chemically distinct outliers.

### Iteration #1

In Supplementary Table S3, the external validation set had the same 19 ligands to estimate the prediction accuracy of the QSAR model. The  $R^2$  value of the best-fit line was 0.05, meaning the QSAR model did not perform well for the given validation set. Visual inspection of Supplementary Figure 11c showed that penthiopyrad, isoflucypram, picarbutrazox, and metominostrobin fell outside the applicability domain of the QSAR model, which would decrease the prediction accuracy of the model. Moreover, penthiopyrad and isoflucypram had fluorine in their chemical structures (Table S1). Penthiopyrad, isoflucypram, and picarbutrazox contained multiple heterocyclic nitrogen atoms. Penthiopyrad, isoflucypram, and metominostrobin had nitrogen-hydrogen structures. To improve the prediction accuracy of the QSAR model, these ligands were removed in the next iteration.

### Iteration #2

After removing penthiopyrad, isoflucypram, picarbutrazox, and metominostrobin in Table S3, the  $R^2$  value of the best-fit line slightly increased. A visual inspection of Supplementary Figure S9 suggested the presence of several outliers (oxathiapirolin, azaconazole, flusulfamide, diethofencarb, and dithianon) that would need to be removed to improve the QSAR model. Oxathiapirolin and flusulfamide had fluorine in their chemical structures (Table S1). Azaconazole and flusulfamide have chlorine in their chemical structures. Diethofencarb had a similar structure to metominostrobin. Only dithianon contained heterocyclic dual sulfur atoms.

### Iteration #3

To further improve the QSAR model, outliers including oxathiapirolin, azaconazole, flusulfamide, diethofencarb, and dithianon were removed from Table S3. The  $R^2$  value of the best-fit line significantly increased from 0.08 to 0.67, indicating those ligands had structural properties that were not predictable using the models (Supplementary Figure S10). The top predictions that would withstand G143A-mutated cytochrome b of *Botrytis cinerea* were fenoxanil (a melanin biosynthesis inhibitor dehydratase), fenpropidin (an amine), iprodione (a dicarboximide), tebufloquin (a 4-quinolyl-acetate), and ametocradin (a QoI). Furametpyr and triazoxide had high predicted affinity, but the difference between their original affinity and predicted affinity was higher than the other four ligands. It should be noted that the model was not able to make accurate predictions when ligands had chlorine, fluorine, and heterocyclic nitrogen atoms in their chemical structures.

### Application of AutoQSR to Predict Fungicides for *Plasmopara viticola* Training Data without a Validation Set

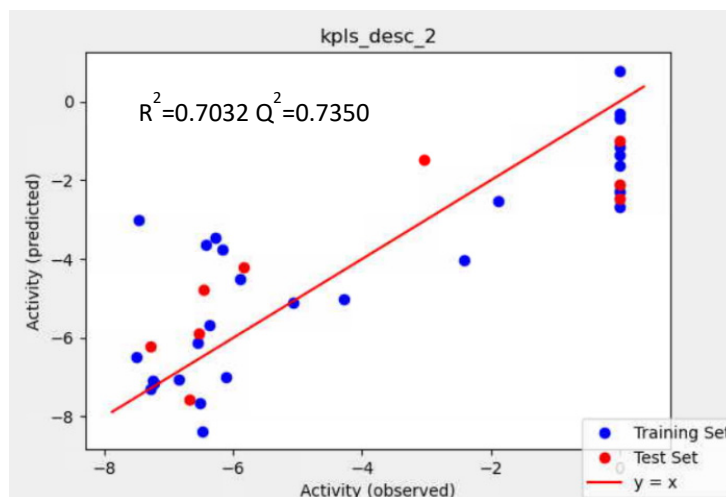
Here, an initial training set was developed using 16 QoI and 20 non-QoI fungicides. The top five QSAR models for *Plasmopara viticola* were kpls\_desc\_2, kpls\_radial\_24, kpls\_linear\_22, kpls\_radial\_22, and pls\_2 (Supplementary Figure S11). The best model was kpls\_desc\_2, generated by kernel partial least squares regression (KPLS) with a desc fingerprint, using the 12th split of the learning set into a test and training set (36 ligands) without a validation set. This model had an S.D. of 1.7498, a  $R^2$  of 0.7032, an RMSE of 1.615, a  $Q^2$  of 0.7350, and a ranking score of 0.7116. In Figure 12a and Supplementary Figure S12, 75% of the ligands occupied the training set and 25% occupied the test set. The scatter plots in Figure 12b and Supplementary Figure S13 indicate that the first four models' training sets correlated closely with the test sets.

Training Set		Test Set	
S.D.	R <sup>2</sup>	RMSE	Q <sup>2</sup>
1.7498	0.7032	1.5615	0.7350

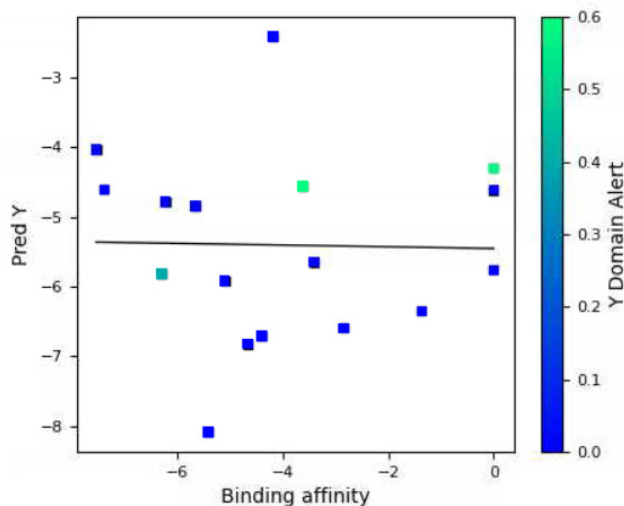
Optimum number of factors = 2

ID Set	Y(Obs)	Y(Pred)	Error	Name
1 test	0.0000	-1.0075	-1.0075	Azoxystrobin
2 train	-6.1770	-3.7677	2.4093	Coumoxystrobin
3 train	0.0000	-0.4428	-0.4428	Enoxastrobin
4 train	-6.3730	-5.6874	0.6856	Fenamidon
5 train	-7.4660	-3.0180	4.4480	Fenaminstrobin
6 train	0.0000	0.7834	0.7834	Fluoxastrobin
7 test	0.0000	-2.1171	-2.1171	Metyltetraprole
8 train	0.0000	-1.6239	-1.6239	Orysastrobin
9 train	0.0000	-2.6921	-2.6921	Picoxystrobin
10 train	0.0000	-1.3514	-1.3514	Pyraclostrobin
11 test	0.0000	-2.4727	-2.4727	pyrametostrobin
12 train	0.0000	-1.1520	-1.1520	Pyraoxystrobin
13 test	-5.8440	-4.2186	1.6254	Pyribencarb
14 train	0.0000	-0.3196	-0.3196	Triclopyricarb
15 train	0.0000	-2.2729	-2.2729	Captan
16 test	-3.0380	-1.4674	1.5706	Ferbam
17 train	-5.8910	-4.4961	1.3949	Folpet
18 train	-1.8780	-2.5294	-0.6514	Mancozeb
19 train	-4.2850	-5.0062	-0.7212	Thiram
20 train	-2.4080	-4.0191	-1.6111	Zineb
21 train	-6.5560	-6.1151	0.4409	Zoxamide
22 train	-6.5160	-7.6569	-1.1409	Sedaxane
23 train	-6.8510	-7.0587	-0.2077	Piperalin
24 train	-6.4860	-8.3683	-1.8823	Inpyrfluxam
25 train	-7.2910	-7.3043	-0.0133	Penconazole
26 test	-6.4640	-4.7788	1.6852	Ferimzone
27 train	-7.5040	-6.4937	1.0103	Cyflufenamid
28 test	-6.5290	-5.8898	0.6392	Diclomezine
29 train	-6.4320	-3.6284	2.8036	Dichlobentiazox
30 train	-6.2790	-3.4461	2.8329	Flufenoxystrobin
31 train	-7.2240	-7.1503	0.0737	Azaconazole
32 train	-6.1090	-7.0061	-0.8971	Fenoxanil
33 train	-7.2400	-7.0895	0.1505	Iprodione
34 test	-7.2910	-6.2103	1.0807	Penthiopyrad
35 test	-6.6800	-7.5782	-0.8982	Oxathiapiprolin
36 train	-5.0670	-5.1204	-0.0534	Metominostrobin

(a)



(b)



(c)

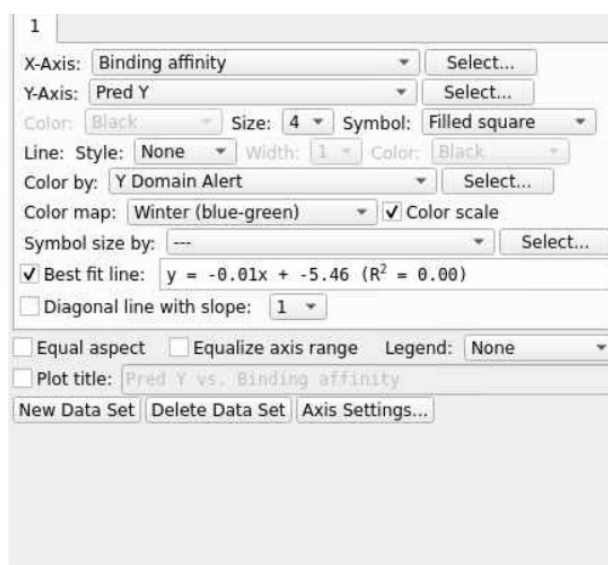


**Figure 12.** (a) Model report for the kpls\_desc\_2 model, (b) scatter plot providing the performance for the kpls\_desc\_2 model, and (c) scatter plot of the prediction set for the top QSAR models in Figure S11 for *Plasmopara viticola* without using a validation set.

Here, in order to evaluate whether the predictions could be improved, it was decided to refine the models by systematically removing outliers that were chemically distinct from the ones that functioned as QoIs and/or when the difference between actual and predicted affinities was larger than 3 kcal/mol, as previously performed.

### Iteration #1

In this iteration, the external validation set had 17 ligands to estimate the prediction accuracy of the QSAR model (Supplementary Table S4). The  $R^2$  value of the best-fit line was not impressive (Figure 12c). Visual inspection of Figure 12c indicated two apparent ligands, fluindapyr and picarbutrazox, falling outside the applicability domain of the QSAR model. Triazoxide, polyoxin, dithianon, and dimoxystrobin also deviated significantly from the regression line. Both fluindapyr and triazoxide had chlorine in their chemical structures (Table S1). Dithianon was the special ligand that had heterocyclic dual sulfur atoms in aromatic rings. Picarbutrazox and dimoxystrobin had a similar structure. Triazoxide and polyoxin showed oxygen with a negative charge. To improve the prediction accuracy of the QSAR model, these ligands were removed in the next iteration.

### Iteration #2

After the first iteration, 6 ligands were removed, and 11 ligands remained in Table S4. Although the  $R^2$  value of the best-fit line increased from 0 to 0.25, there were still some outliers, such as furametpyr, fenpropidin, and tebufloquin, shown in Supplementary Figure S14. Furametpyr had chlorine that was similar to triazoxide in Table S1. Tebufloquin had fluorine that was similar to fluindapyr. All three ligands (furametpyr, fenpropidin, and tebufloquin) had a similar carbon structure, as shown in Table S1. To further improve accuracy, these ligands were removed in the next iteration.

### Iteration #3

After removing the outliers mentioned in the second iteration in Table S4, the  $R^2$  value of the best-fit line (Supplementary Figure S15) became 0.63, with an acceptable prediction accuracy. The top predictions that would withstand G143A-mutated cytochrome b of *Plasmopara viticola* were flusulfamide (a benzene-sulfonamide), ametotradin (a QoI), ethaboxam (a thiazole carboxamide), and famoxadone (a QoI). Isoflucypram and diethofencarb showed high predicted affinity with low original affinity; thus, they were not an appropriate validation set for the QSAR prediction model. Outliers for this QSAR model carried fluorine, chlorine, and oxygen with a charge, and an aromatic ring with sulfur.

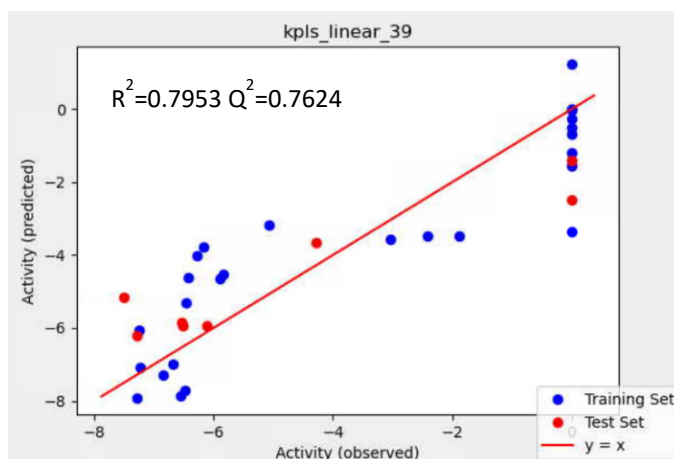
### Training Data with a Validation Set

In this case, two QoI fungicides, fenaminstrobin and fenamidone, were assigned as the validation set for the QSAR models. Consequently, there were 34 ligands used for the QSAR model (Figure 13a and Supplementary Figure S17). The ranking scores for the top five QSAR models with a validation set (Supplementary Figure S16) were higher than for the model without a validation set. The results of the QSAR models from both *Botrytis cinerea* and *Plasmopara viticola* showed that a validation set may provide more accurate prediction models. The top QSAR models shown for *Plasmopara viticola* in Supplementary Figure S16 were kpls\_linear\_39, kpls\_desc\_31, kpls\_dendritic\_31, kpls\_linear\_2, and kpls\_linear\_31. The best model was kpls\_linear\_39, which was generated by kernel partial least squares regression (KPLS) with a linear fingerprint, using the 39th split of the learning set into a test and training set (34 ligands) with a validation set. This model had an S.D. of 1.4315, a  $R^2$  of 0.7953, an RMSE of 1.4160, a  $Q^2$  of 0.7624, and a ranking score of 0.7733. As seen in the scatter plots in Figure 13b and Supplementary Figure S18, the pattern of training sets was similar to the plots in Figures 12b and S13.

Training Set		Test Set	
S.D.	R <sup>2</sup>	RMSE	Q <sup>2</sup>
1.4315	0.7953	1.4160	0.7624

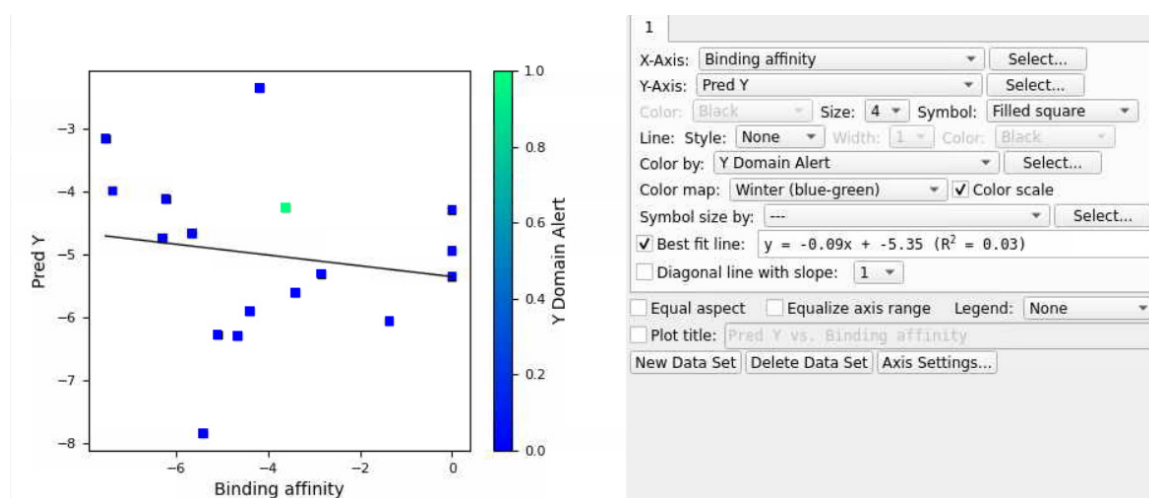
Optimum number of factors = 1

ID Set	Y(Obs)	Y(Pred)	Error	Name
1 test	0.0000	-2.4836	-2.4836	Azoxystrobin
2 train	-6.1770	-3.7671	2.4099	Coumoxystrobin
3 train	0.0000	0.0155	0.0155	Enoxastrobin
4 train	0.0000	-1.5633	-1.5633	Fluoxastrobin
5 train	0.0000	-0.4981	-0.4981	Metyltetraprole
6 train	0.0000	-1.1987	-1.1987	Orysastrobin
7 train	0.0000	-0.2746	-0.2746	Picoxystrobin
8 train	0.0000	1.2507	1.2507	Pyraclostrobin
9 test	0.0000	-1.4058	-1.4058	pyrametostrobin
10 train	0.0000	-0.0120	-0.0120	Pyraoxystrobin
11 train	-5.8440	-4.5273	1.3167	Pyribencarb
12 train	0.0000	-0.6917	-0.6917	Triclopyricarb
13 train	0.0000	-3.3722	-3.3722	Captan
14 train	-3.0380	-3.5565	-0.5185	Ferbam
15 train	-5.8910	-4.6459	1.2451	Folpet
16 train	-1.8780	-3.4678	-1.5898	Mancozeb
17 test	-4.2850	-3.6604	0.6246	Thiram
18 train	-2.4080	-3.4678	-1.0598	Zineb
19 train	-6.5560	-7.8529	-1.2969	Zoxamide
20 test	-6.5160	-5.9292	0.5868	Sedaxane
21 train	-6.8510	-7.2809	-0.4299	Piperalin
22 train	-6.4860	-7.7241	-1.2381	Inpyrfluxam
23 test	-7.2910	-6.2129	1.0781	Penconazole
24 train	-6.4640	-5.3040	1.1600	Ferimzone
25 test	-7.5040	-5.1571	2.3469	Cyflufenamid
26 test	-6.5290	-5.8468	0.6822	Diclomezine
27 train	-6.4320	-4.6090	1.8230	Dichlobentiazox
28 train	-6.2790	-4.0203	2.2587	Flufenoxystrobin
29 train	-7.2240	-7.0790	0.1450	Azaconazole
30 test	-6.1090	-5.9480	0.1610	Fenoxanil
31 train	-7.2400	-6.0749	1.1651	Iprodione
32 train	-7.2910	-7.9161	-0.6251	Penthiopyrad
33 train	-6.6800	-6.9772	-0.2972	Oxathiapiprolin
34 train	-5.0670	-3.1909	1.8761	Metominostrobin



(a)

(b)



(c)

**Figure 13.** (a) Model report of the kpls\_linear\_39 model, (b) scatter plot providing the performance of the kpls\_linear\_39 model, and (c) scatter plot of the prediction set for the top QSAR models in Figure S16 for *Plasmopara viticola* using a validation set.

#### Iteration #1

The predicted binding affinities in Supplementary Table S5 were slightly lower than those in Table S4. The  $R^2$  value of the best-fit line was 0.03, as shown in Supplementary Figure S13c. Visual inspection of Figure 13c identified three apparent ligands (fluindapyr, picarbutrazox, and dimoxystrobin) falling outside the applicability domain of the QSAR model, which affected the prediction accuracy of the QSAR model. Dithianon was another ligand that lay further from the regression line, and it was the only ligand that contained an aromatic ring with sulfur (Table S1). Fluindapyr and picarbutrazox had similar aromatic

rings. To improve the prediction accuracy of the QSAR model, these ligands were removed during the next iteration.

#### Iteration #2

After the first iteration, 4 ligands were removed, and 13 ligands remained in Table S5. The  $R^2$  value of the best-fit line shown in Figure S19 improved from 0.03 to 0.16 in this iteration (Supplementary Figure S19). Furametpyr, flusulfamide, tebufloquin, triazoxide, polyoxin, famoxadone, and mandestrobin were outliers based on visual inspection. Furametpyr, flusulfamide, and triazoxide had chlorine. Flusulfamide and tebufloquin had fluorine in their ligand structures (Table S1). Both triazoxide and polyoxin had oxygen with a charge in their ring structures. Famoxadone and mandestrobin had a similar structure to dimoxystrobin. For further improvement of the model, these ligands were removed.

#### Iteration #3

In this case, the  $R^2$  value of the best-fit line shown in Figure S20 was 0.64, meaning the prediction accuracy of the QSAR models was acceptable. The top predictions that would withstand G143A-mutated cytochrome b of *Plasmopara viticola* were fenpropidin (an amine), ametoctradin (a QoI), and ethaboxam (a thiazole carboxamide). Isoflucypram, diethofencarb, and fluoxapiprolin were not appropriate selections since their predicted affinities were very different from their original affinities (Table S5). Outliers for this QSAR model also contained fluorine and chlorine, similar to the QSAR model with a validation set.

## 4. Discussion

The primary purpose of this study was to use in silico simulations to select the highest affinity QoI fungicides for the cytochrome b targets of *Plasmopara viticola* and *Botrytis cinerea*. Based on different in silico simulation methods that consisted of generalized and site-directed ligand impingement methods, docking simulations showed ubiquinol to be the highest affinity ligand for cytochrome b, regardless of the sourced organism. Ubiquinol is bound to cytochrome b primarily via hydrophobic interactions.

In the case of WT cytochrome b of *Plasmopara viticola*, mandestrobin, fenaminstrobin, dimoxystrobin, fenamidone, famoxadone, and ametoctradin bound with the highest affinity and were thus considered effective fungicides. They were also effective agents against G143A-mutated cytochrome b. Coumoxystrobin, flufenoxystrobin, and pyribencarb showed a strongly poor affinity toward WT and the G143A-mutated version, suggesting their susceptibility to potential resistance. As a resistant fungicide, azoxystrobin did not bind to WT and G143A-mutated cytochrome b as expected. Although folpet, a low-risk FRAC code fungicide, showed a reasonable affinity toward G143A-mutated cytochrome b, only thiram had stable and strong affinities toward both WT and G143A-mutated types of cytochrome b among the selected low-risk fungicides. According to the general analysis, from the high- and low-risk groups, mandestrobin, fenaminstrobin, dimoxystrobin, famoxadone, fenamidone, ametoctradin, and thiram emerged as those with the strongest affinity toward *Plasmopara viticola* cytochrome b.

Pyribencarb, mandestrobin, fenamidone, famoxadone, and ametoctradin were effective agents against WT and G143A-mutated cytochrome b of *Botrytis cinerea*. While pyraoxystrobin and metominostrobin had a strong affinity toward WT cytochrome b, their affinity was poor toward mutated cytochrome b. The low-risk fungicides, folpet and captan, had a strong affinity with WT cytochrome b but did not bind to G143A-mutated versions of *Botrytis cinerea* cytochrome b. Thiram showed consistent but moderate affinities.

According to the binding affinity simulation analysis, mandestrobin emerged as the top binder for both *Plasmopara viticola* and *Botrytis cinerea* cytochrome b, regardless of common mutations. Thiram, on the other hand, emerged as a reasonable, low-risk fungicide that worked on WT and the G143A-mutated versions of both fungi. However, the affinity analysis clearly indicated the difficulty of making such broad-spectrum recommendations because of the peculiarities of cytochrome b proteins within different organisms.

Based on a QSAR analysis with an extended array of fungicides, fenpropidin (an amine), fenoxanil (a melanin biosynthesis inhibitor dehydratase), isoflucypram (a succinate dehydrogenase inhibitor), and ametoctradin (a QoI) emerged as effective against G143A-mutated cytochrome b of *Botrytis cinerea*. Moreover, fenoxanil, fenpropidin, iprodione (a dicarboximide), tebufloquin (a 4-quinolyl-acetate), and ametoctradin emerged as high-affinity inhibitors in an analysis with a secondary validation set. The QSAR analysis without a validation set revealed flusulfamide (a benzene-sulfonamide), ametoctradin, ethaboxam (a thiazole carboxamide), and famoxadone (a QoI) emerged as high-affinity fungicides on G143A-mutated cytochrome b of *Plasmopara viticola*. Moreover, fenpropidin, ametoctradin, and ethaboxam showed a strong affinity in the analysis with a secondary validation set. Based on both the docking simulations and QSAR analysis, ametoctradin emerged as a potential high-affinity QoI fungicide toward the G143A-mutated cytochrome b.

## 5. Conclusions

It was observed that mandestrobin, fenaminstrobin, dimoxystrobin, fenamidone, and famoxadone bound to the WT, whereas dimoxystrobin and fenaminstrobin bound to the G143A-mutated cytochrome b of *Plasmopara viticola* with the highest affinity. Although the low-risk fungicide folpet showed reasonable affinity toward G143A-mutated cytochrome b, only thiram had stable and strong affinities toward both WT and G143A-mutated types of cytochrome b among the selected low-risk fungicides. In general, from the high- and low-risk groups, dimoxystrobin, fenaminstrobin, and thiram showed the strongest affinity toward *Plasmopara viticola* cytochrome b. Pyribencarb, mandestrobin, enoxastrobin, and pyraoxystrobin had a high affinity toward WT, whereas famoxadone, mandestrobin, pyribencarb, picoxystrobin, and metominostrobin bound tightly to G143A-mutated cytochrome b of *Botrytis cinerea*. Folpet and captan had a strong affinity with WT cytochrome b but did not bind to G143A-mutated versions of *Botrytis cinerea* cytochrome b. Thiram showed consistent but moderate affinities. Mandestrobin emerged as the top binder for both WT *Plasmopara viticola* and WT *Botrytis cinerea* cytochrome b. Famoxadone appeared to be a versatile binder for G143A-mutated cytochrome b of both *Plasmopara viticola* and *Botrytis cinerea*. Thiram emerged as a reasonable, low-risk non-QoI fungicide that works on WT and G143A-mutated versions of both fungi. QSAR analysis revealed fenpropidin, fenoxanil, and ethaboxam non-QoIs to have a high affinity for G143A-mutated cytochrome b of *Plasmopara viticola* and *Botrytis cinerea*. It is recommended that modeling results be experimentally validated via in vitro and/or plant field studies while attempting to improve the accuracy of the QSAR model using the experimental (validation) data.

**Supplementary Materials:** The following supporting information can be downloaded at: <https://www.mdpi.com/article/10.3390/microorganisms11051341/s1>, Table S1. Compound information for all the fungicides; Table S2. Calculated binding affinity (via docking simulations) and predicted binding affinity between 19 selected ligands and G143A-mutated cytochrome b of *Botrytis cinerea* without a validation set; Table S3. Calculated binding affinity (via docking simulations) and predicted binding affinity between 19 selected ligands and G143A-mutated cytochrome b of *Botrytis cinerea* for the QSAR model with a validation set; Table S4. Calculated binding affinity (via docking simulations) and predicted binding affinity between 17 selected ligands and G143A-mutated cytochrome b of *Plasmopara viticola* without a validation set; Table S5. Calculated binding affinity (via docking simulations) and predicted binding affinity between 17 selected ligands and G143A-mutated cytochrome b of *Plasmopara viticola* by using the QSAR model with a validation set; Figure S1. Top 10-ranked QSAR models without a validation set for (fungicides used in) *Botrytis cinerea*; Figure S2. Model reports for (a) in the main article (b) kpls\_radial\_19, (c) kpls\_dendritic\_19, (d) kpls\_desc\_19, and (e) kpls\_linear\_19 models of *Botrytis cinerea* without using the validation set; Figure S3. Scatter plot about performance for (a) main article (b) kpls\_radial\_19, (c) kpls\_dendritic\_19, (d) kpls\_desc\_19, and (e) kpls\_linear\_19 models of *Botrytis cinerea* without using the validation set; Figure S4. Scatter plot of the external validation set after removing four outliers in Figure 10c; Figure S5. Scatter plot of the external validation set after removing four outliers in Figure S4; Figure S6. Top 10-ranked QSAR model reports with validation sets for *Botrytis cinerea*; Figure S7. Model reports for (a) main

article (b) kpls\_radial\_19, (c) kpls\_dendritic\_19, (d) kpls\_desc\_19, and (e) kpls\_linear\_19 models of *Botrytis cinerea* using the validation set; Figure S8. Scatter plot about performance for (a) main article (b) kpls\_radial\_8, (c) kpls\_linear\_30, (d) kpls\_dendritic\_30, and (e) kpls\_dendritic\_39 models of *Botrytis cinerea* using the validation set; Figure S9. Scatter plot of the external validation set after removing four outliers in Figure 11c; Figure S10. Scatter plot of the external validation set after removing five outliers in Figure S9; Figure S11. Top 10-ranked QSAR model reports without the validation set for *Plasmopara viticola*; Figure S12. Model reports for (a) main article (b) kpls\_radial\_24, (c) kpls\_linear\_22, (d) kpls\_radial\_22, and (e) pls\_2 models of *Plasmopara viticola* without using the validation set; Figure S13. Scatter plot about performance for (a) main article (b) kpls\_radial\_24, (c) kpls\_linear\_22, (d) kpls\_radial\_22, and (e) pls\_2 models of *Plasmopara viticola* without using the validation set; Figure S14. Scatter plot of external validation set for all top five models after removing six outliers in Figure 12c; Figure S15. Scatter plot of external validation set for all top five models after removing three outliers in Figure S14; Figure S16. Top 10-ranked QSAR model reports with the validation set for *Plasmopara viticola*; Figure S17. Model reports for (a) main article (b) kpls\_desc\_31, (c) kpls\_dendritic\_39, (d) kpls\_linear\_2, and (e) kpls\_linear\_31 models of *Plasmopara viticola* using the validation set; Figure S18. Scatter plot about performance for (a) main article (b) kpls\_desc\_31, (c) kpls\_dendritic\_39, (d) kpls\_linear\_2, and (e) kpls\_linear\_31 models of *Plasmopara viticola* using the data set; Figure S19. Scatter plot of the external validation set after removing four outliers in Figure 13c; Figure S20. Scatter plot of the external validation set after removing seven outliers in Figure S19.

**Author Contributions:** J.Z. conducted the simulations and prepared the manuscript. S.D.F. conceived the idea(s), directed the studies, co-authored, and reviewed the manuscript. All authors have read and agreed to the published version of the manuscript.

**Funding:** Portions of this work were funded by Texas A&M AgriLife Research.

**Data Availability Statement:** The data supporting the findings of this study are available from the corresponding author SF on request.

**Acknowledgments:** The authors acknowledge the support provided by Texas A&M University's High-Performance Research Computing Center (HPRC) to conduct all the simulations.

**Conflicts of Interest:** The authors declare no conflict of interest associated with the work herein.

## Abbreviations

QoI—Quinone outside inhibitor; MOA—mode of action; WT—wild type (WT); G143A—Glycine 143 to Alanine; QSAR—quantitative structure–activity relationship; ATP—Adenosine Triphosphate; FRAC—Fungicide Resistance Action Committee; OPLS3—Optimized Potentials for Liquid Simulations 3; AutoQSAR—Schrödinger automated quantitative structure–activity relationship; AI—Artificial Intelligence; MLR—multiple linear regression; PLS—partial least-squares regression; KPLS—kernel-based partial least-squares regression; PCR—principal components regression; QSQE—Quaternary Structure Quality Estimate; GMQE—Global Model Quality Estimate.

## References

1. FAO. *FAOSTAT Statistical Database*; Food and Agriculture Organization of the United Nations: Roma, Italy, 2020.
2. Kramer, J.; Simnitt, S.; Calvin, L. Fruit and Tree Nuts Outlook: September 2021. *US Dept. Agr. Econ. Res. Serv.* **2021**, *2021*, 37.
3. Murray, R.E.; Candan, A.P.; Vazquez, D.E. *Manual de Poscosecha de Frutas: Manejo Integrado de Patógenos*; Ediciones INTA: Buenos Aires, Argentina, 2019.
4. Kassemeyer, H.-H. Fungi of grapes. In *Biology of Microorganisms on Grapes, in Must and in Wine*; Springer: Berlin/Heidelberg, Germany, 2017; pp. 103–132.
5. Caffi, T.; Rossi, V.; Carisse, O. Evaluation of a dynamic model for primary infections caused by *Plasmopara viticola* on grapevine in Quebec. *Plant Health Prog.* **2011**, *12*, 22. [[CrossRef](#)]
6. Agrios, G.N. *Plant Pathology*; Elsevier: Amsterdam, The Netherlands, 2005.
7. Mezei, I.; Lukić, M.; Berbakov, L.; Pavković, B.; Radovanović, B. Grapevine Downy Mildew Warning System Based on NB-IoT and Energy Harvesting Technology. *Electronics* **2022**, *11*, 356. [[CrossRef](#)]

8. Chen, W.-J.; Delmotte, F.; Cervera, S.R.; Douence, L.; Greif, C.; Corio-Costet, M.-F. At least two origins of fungicide resistance in grapevine downy mildew populations. *Appl. Environ. Microbiol.* **2007**, *73*, 5162–5172. [[CrossRef](#)] [[PubMed](#)]
9. Dean, R.; Van Kan, J.A.; Pretorius, Z.A.; Hammond-Kosack, K.E.; Di Pietro, A.; Spanu, P.D.; Rudd, J.J.; Dickman, M.; Kahmann, R.; Ellis, J. The Top 10 fungal pathogens in molecular plant pathology. *Mol. Plant Pathol.* **2012**, *13*, 414–430. [[CrossRef](#)] [[PubMed](#)]
10. Elmer, P.; Reglinski, T. Biosuppression of *Botrytis cinerea* in grapes. *Plant Pathol.* **2006**, *55*, 155–177. [[CrossRef](#)]
11. Foster, A.J. Identification of fungicide targets in pathogenic fungi. *Physiol. Genet.* **2018**, *15*, 277–296.
12. Bartlett, D.W.; Clough, J.M.; Godwin, J.R.; Hall, A.A.; Hamer, M.; Parr-Dobrzanski, B. The strobilurin fungicides. *Pest Manag. Sci. Former. Pestic. Sci.* **2002**, *58*, 649–662. [[CrossRef](#)]
13. Hahn, M. The rising threat of fungicide resistance in plant pathogenic fungi: *Botrytis* as a case study. *J. Chem. Biol.* **2014**, *7*, 133–141. [[CrossRef](#)]
14. Samuel, S.; Papayiannis, L.C.; Leroy, M.; Veloukas, T.; Hahn, M.; Karaoglanidis, G.S. Evaluation of the incidence of the G143A mutation and cytb intron presence in the cytochrome bc-1 gene conferring QoI resistance in *Botrytis cinerea* populations from several hosts. *Pest Manag. Sci.* **2011**, *67*, 1029–1036. [[CrossRef](#)]
15. Hollomon, D.W. Fungicide resistance: Facing the challenge—A review. *Plant Prot. Sci.* **2015**, *51*, 170–176. [[CrossRef](#)]
16. Sierotzki, H.; Kraus, N.; Assemet, P.; Stanger, C.; Cleere, S.; Windass, J.; Gisi, U. Evolution of resistance to QoI fungicides in *Plasmopara viticola* populations in Europe. In Proceedings of the Modern Fungicides and Antifungal Compounds IV: 14th International Reinhardtsbrunn Symposium, Friedrichroda, Germany, 25–29 April 2004; pp. 73–80.
17. Lijuan, X.; Shangfei, Q.; Zhengchuan, S.; Huiling, Y. Field efficacy of the combination of famoxadone and metalaxyl-M against *Plasmopara viticola* and the residue dynamics of the two fungicides in grape. *Chin. J. Pestic. Sci.* **2022**, *24*, 326–331.
18. Kabade, S.H.; Pawar, S.B.; Edoliya, R.; Saha, S. Performance and Phytotoxicity assessment of Mancozeb 40%+ Azoxystrobin 7% OS against downy mildew of grapes in Maharashtra, India. *J. Mycopathol. Res.* **2022**, *60*, 581–585. [[CrossRef](#)]
19. Liu, F.; Li, J.; Li, H.; Wang, K.; Meng, L.; Li, B.; Mu, W.; Liu, F. Evaluation on Synergistic Activity and Resistance Development of the Mixture of Iprodione and Fluopyram Against *Botrytis cinerea*. Available online: <https://ssrn.com/abstract=4118573> (accessed on 1 April 2023).
20. Sagar, N.; Jamadar, M.; Shalini, N.; Jagginavar, S.; Pattar, P. Bioefficacy of different fungicides against *Plasmopara viticola* and *Erysiphe necator* of grapes. *Pharma Innov. J.* **2022**, *11*, 2512–2518.
21. Malandrakis, A.A.; Kavroulakis, N.; Chrysikopoulos, C.V. Synergy between Cu-NPs and fungicides against *Botrytis cinerea*. *Sci. Total Environ.* **2020**, *703*, 135557. [[CrossRef](#)]
22. Arnold, K.; Bordoli, L.; Kopp, J.; Schwede, T. The SWISS-MODEL workspace: A web-based environment for protein structure homology modelling. *Bioinformatics* **2006**, *22*, 195–201. [[CrossRef](#)]
23. Maldonado, M.; Guo, F.; Letts, J.A. Atomic structures of respiratory complex III<sub>2</sub>, complex IV, and supercomplex III<sub>2</sub>-IV from vascular plants. *Elife* **2021**, *10*, e62047. [[CrossRef](#)]
24. Waterhouse, A.; Bertoni, M.; Bienert, S.; Studer, G.; Tauriello, G.; Gumienny, R.; Heer, F.T.; de Beer, T.A.P.; Rempfer, C.; Bordoli, L. SWISS-MODEL: Homology modelling of protein structures and complexes. *Nucleic Acids Res.* **2018**, *46*, W296–W303. [[CrossRef](#)]
25. Colovos, C.; Yeates, T.O. Verification of protein structures: Patterns of nonbonded atomic interactions. *Protein Sci.* **1993**, *2*, 1511–1519. [[CrossRef](#)]
26. Pontius, J.; Richelle, J.; Wodak, S.J. Deviations from standard atomic volumes as a quality measure for protein crystal structures. *J. Mol. Biol.* **1996**, *264*, 121–136. [[CrossRef](#)]
27. Irwin, J. ZINC15. docking. org: Over 1.5 billion compounds you can search and buy; 550 million lead-like you can dock. In Proceedings of the Abstracts of Papers of the American Chemical Society, Washington, DC, USA, 15–16 September 2019; Volume 257.
28. Kim, S.; Chen, J.; Cheng, T.; Gindulyte, A.; He, J.; He, S.; Li, Q.; Shoemaker, B.A.; Thiessen, P.A.; Yu, B. PubChem in 2021: New data content and improved web interfaces. *Nucleic Acids Res.* **2021**, *49*, D1388–D1395. [[CrossRef](#)] [[PubMed](#)]
29. Jorgensen, W.L.; Tirado-Rives, J. The OPLS [optimized potentials for liquid simulations] potential functions for proteins, energy minimizations for crystals of cyclic peptides and crambin. *J. Am. Chem. Soc.* **1988**, *110*, 1657–1666. [[CrossRef](#)] [[PubMed](#)]
30. Release, S. *AutoQSAR*; Schrödinger, LLC: New York, NY, USA, 2022.
31. Laskowski, R.A.; Rullmann, J.A.C.; MacArthur, M.W.; Kaptein, R.; Thornton, J.M. AQUA and PROCHECK-NMR: Programs for checking the quality of protein structures solved by NMR. *J. Biomol. NMR* **1996**, *8*, 477–486. [[CrossRef](#)] [[PubMed](#)]
32. Williams, C.J.; Headd, J.J.; Moriarty, N.W.; Prisant, M.G.; Videau, L.L.; Deis, L.N.; Verma, V.; Keedy, D.A.; Hintze, B.J.; Chen, V.B. MolProbity: More and better reference data for improved all-atom structure validation. *Protein Sci.* **2018**, *27*, 293–315. [[CrossRef](#)]
33. Grasso, V.; Palermo, S.; Sierotzki, H.; Garibaldi, A.; Gisi, U. Cytochrome b gene structure and consequences for resistance to Qo inhibitor fungicides in plant pathogens. *Pest Manag. Sci. Former. Pestic. Sci.* **2006**, *62*, 465–472. [[CrossRef](#)]
34. Mounkoro, P.; Michel, T.; Benhachemi, R.; Surpateanu, G.; Iorga, B.I.; Fisher, N.; Meunier, B. Mitochondrial complex III Qi-site inhibitor resistance mutations found in laboratory selected mutants and field isolates. *Pest Manag. Sci.* **2019**, *75*, 2107–2114. [[CrossRef](#)]
35. Wong, F.P.; Wilcox, W.F. Distribution of baseline sensitivities to azoxystrobin among isolates of *Plasmopara viticola*. *Plant Dis.* **2000**, *84*, 275–281. [[CrossRef](#)]

36. Fisher, N.; Meunier, B.; Biagini, G.A. The cytochrome bc1 complex as an antipathogenic target. *Febs Lett.* **2020**, *594*, 2935–2952. [[CrossRef](#)]
37. Wenz, T.; Covian, R.; Hellwig, P.; MacMillan, F.; Meunier, B.; Trumpower, B.L.; Hunte, C. Mutational analysis of cytochrome b at the ubiquinol oxidation site of yeast complex III. *J. Biol. Chem.* **2007**, *282*, 3977–3988. [[CrossRef](#)]

**Disclaimer/Publisher’s Note:** The statements, opinions and data contained in all publications are solely those of the individual author(s) and contributor(s) and not of MDPI and/or the editor(s). MDPI and/or the editor(s) disclaim responsibility for any injury to people or property resulting from any ideas, methods, instructions or products referred to in the content.